Energetic ion, atom, and molecule reactions and excitation in low-current H_2 discharges: Model

A. V. Phelps
JILA, National Institute of Standards and Technology and University of Colorado, Boulder, Colorado 80309-0440, USA
(Received 4 March 2009; published 3 June 2009)

Models of the elastic, inelastic, and reactive collisions of energetic hydrogen ions, atoms, and molecules are developed for predicting H_α and H_2 near-uv emission, H_α Doppler profiles, and ion energy distributions for low-pressure, low-current discharges in H_2. The model is applied to spatially uniform electric field E to gas density N ratios of 350 Td$\leq E/N \leq$45 kTd and $8\times10^{19}\leq Nd\leq 10\times10^{21}$ m^{-2}, where d is the electrode separation and 1 Td$=10^{-21}$ V m^2. Mean ion energies at the cathode are 5–1500 eV. Cross sections for H^+, H_2^+, H_3^+, H, H_2, and excited H($n=3$) collisions with H_2 and reflection probabilities from electrodes are updated and summarized. Spatial and energy distributions of ions and fast neutrals are calculated using a "multibeam" technique. At the lower E/N and Nd, electron excitation of H_α dominates near the anode. Excitation of H_α by fast H atoms near the cathode increases rapidly with pressure through a multistep reaction sequence. At higher E/N, fast H atoms produced at the cathode surface excite much of the H_α. The model agrees with experimental spatial distributions of H_α emission and Doppler profiles. Ion energy distributions agree with experiments only for H_2^+. Cross sections are derived for excitation of the near-uv continuum of H_2 by H atoms.

DOI: 10.1103/PhysRevE.79.066401 PACS number(s): 52.20.−j, 52.80.Dy, 34.50.Gb

I. INTRODUCTION

The objectives of this paper are to provide detail and to update our earlier model [1] of the spatial and spectral distribution of H_α emission in low-current uniform-field discharges in H_2 for comparison with experiments reported briefly [1] and in detail separately [2–4]. Because the complexity of the ion-molecule-surface reaction scheme makes it difficult to infer the important collision processes directly from measurements, we are presenting the model before the experiment. Known collision cross sections are summarized and assumptions regarding unknown cross sections are specified. The model generally agrees well with experiments.

The study of very-low-current discharges makes possible the determination and/or testing of volume and surface reaction rate coefficients and probabilities under relatively simple conditions. For these discharges, called "Townsend" or dark discharges, Townsend's model of an exponential growth of ionization by an electron avalanche in a uniform electric field is a good approximation [5–9]. At the lower current densities space-charge electric fields are small and are neglected. As the current density increases space charge is responsible for the onset of nonlinear gas-ionization and electrode phenomena that result in instabilities [8]. Such nonlinear phenomena are more important at the higher current densities of glow discharges, where space-charge-field effects greatly complicate the models [5–7]. Evidence for the need to examine low-current density discharges is the considerable confusion regarding the proper application of basic data, such as collision cross sections for elastic scattering, charge transfer, and momentum transfer, in models of ion transport and gas heating caused by ions and neutral atoms in the cathode region [10].

The complexity of models of hydrogen discharges has increased with the recognition of the role of ion-molecule reactions and of fast neutral species in the production of electrons at the cathode and of photons in the gas [1,11–13]. Also of importance for this paper are the conclusions as to the roles of H_3^+ ions [14–18] and of fast atoms [11,13,15,19–21] in glow discharges. Some of the more important investigations for modeling purposes are as follows.

McClure and Granzow [22,23] modeled 80 kV discharges and measured cross sections for 3–120 keV. Their model considered only H^+ and H_2^+, but they measured cross sections for collisions of H_3^+ with H_2.

Hantzsche [11] and Emeleus and Coulter [13] modeled light from cathode fall considering excitation by electrons and hydrogen ions and neutrals. At high voltages (5 and 10 kV) and very-low pressures (<1 mTorr), they attributed most of the light to excitation by ions. The peak emission near the cathode is attributed to the maximum in the electron excitation cross section—a conclusion with which we disagree. At 500 V and below and $pd\sim0.2$ Torr cm, they predicted that excitation by hydrogen ions and atoms is significantly smaller than electron excitation.

Dexter *et al.* [14] used Monte Carlo techniques to develop a self-consistent model of the abnormal hydrogen cathode fall at an average E/N of ≈2.5 kTd and $pd_c=0.6$ Torr cm, where d_c is the cathode fall thickness and 1 Td $=10^{-21}$ V m^2. Using rather approximate cross sections for ion-H_2 collisions, they compared calculated and measured energy distributions of H^+, H_2^+, and H_3^+ at the cathode and found fair agreement except at low energies. Some of the disagreement is probably caused by their assumption of rapid $H^+ + 2H_2 \rightarrow H_3^+ + H_2$ reactions in spite of their low pressures [24].

Heim and Störi [15] modeled the sheath between the negative glow of a hollow cathode and an energy analyzer electrode versus extraction voltage (35–130 V, $d_c\approx3$ mm, and $p\sim1$ Torr). They neglected angular scattering. In order to fit to experiment, their model requires very small cross sections ($\ll10^{-20}$ m^2) for breakup in $H_3^+ + H_2$ collisions—a conclusion with which we will disagree.

Bretagne and co-workers [16,19–21] used Monte Carlo and convective mathematical techniques to model the reactions and drift of H^+, H_2^+, and H_3^+ in uniform electric fields for $10<E/N<600$ Td. By fitting ion mobilities and ion en-

ergy distributions, they determined energy-dependent momentum transfer and breakup cross sections for $H_3^+ + H_2$ collisions. Of particular interest is their assumed differential scattering cross section and resultant large contributions of rotational and vibrational excitation to the effective momentum transfer cross section for $H^+ + H_2$ collisions.

Early observations of Doppler broadening of H_α in rf and dc glow discharges by Cappelli *et al.* [25] and by Ayers and Benesch [26] were followed by the measurements of line profiles and spatial distributions by Barbeau and Jolly [12], Lavrov and Melinkov [27], Radovanov *et al.* [28], and Konjević and co-workers [29]. Because of the spatially nonuniform electric fields, we will postpone the application of our model to these experiments [30]. We briefly cite the relation of the present work to H_α emission from the outer planets [31,32], plasma fusion related devices [33,34], and the "hydrino" question [35–38].

The spatial dependencies and Doppler profiles for the H_α line emission observed by Petrović *et al.* [1] led to the proposal that the excitation is the result of sequential reactions that begin with electron impact ionization of H_2 to produce H_2^+ and eventually produce H_α excitation in fast H atom collisions with H_2. The measured H_α Doppler profiles demonstrated that the component of the Doppler profile emitted by excited $H(n=3)$ atoms approaching the cathode extends to velocities corresponding to acceleration of H^+ to the applied voltage, while the components of the Doppler profile emitted by excited H atoms leaving the cathode are strongly dependent on cathode material.

More recently, Stokic *et al.* [39] presented additional spatial distributions of H_α emission, with emphasis on the absolute calibration of the emission and analysis of the ionization and excitation by electrons. In the present series of papers, we are concerned with the variation in the excitation of H_α and of the H_2 near-uv continuum with electric field, gas density, and current density [2]; surface reflection models; the improvement of collision cross sections [40]; comparisons of the models of H_α Doppler profiles with experiment [3]; and the correlations of transient current and emission data with our steady-state model [4].

The cross sections for collisions with H_2 used in our model are reviewed in Sec. III. A more detailed discussion is presented in Ref. [40]. The model for calculating the spatially dependent emission is described in Sec. IV. The spatially and energy-dependent results are used to calculate Doppler profiles in Sec. V. Illustrative comparisons are made with experiments.

II. OVERVIEW OF MODEL

Reactive collision processes of importance in the model of this paper are shown in the schematic of Fig. 1. The arrows show the reactive collision processes considered for the ions and fast neutrals approaching the cathode at a high E/N of 10 kTd [1] and at a low E/N of 350 Td. The numbers associated with the reactions are number of reactions per electron reaching the anode, i.e., they are the products of the hydrogen species flux normalized to the electron flux at the anode and the probability of reaction averaged over space

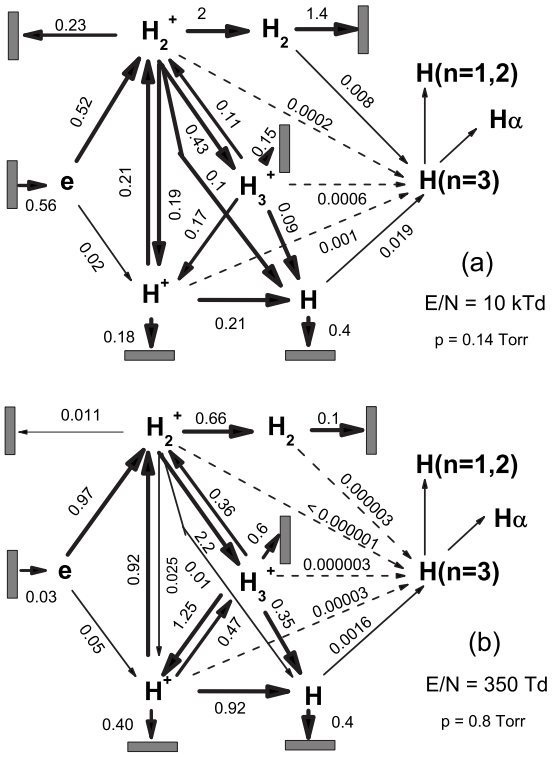

FIG. 1. Schematic of reactive collision processes of importance in our model of H_α emission for (a) $E/N=10$ kTd and $p=0.14$ Torr and (b) $E/N=350$ Td and $p=0.80$ Torr. The numbers give the calculated number of reactions of a given type that occur in the drift tube per electron reaching the anode. Arrows ending on shaded boxes represent loss to the cathode. The width of the solid arrows indicates the relative number of reactions. The light dashed arrows indicate very slow reactions. This diagram is only for species moving toward the cathode.

using the numerical solutions of Sec. IV. The numbers indicating electrode and wall losses are normalized to the electron flux at the anode. Thus, these numbers in Fig. 1 are a measure of the importance of each process. We do not show numbers for elastic collisions and inelastic collisions [41] or for the fast H atoms produced at the cathode and moving toward the anode.

The diagrams of Fig. 1 show that at E/N of 10 kTd and 350 Td the H_2^+ produced by electron impact on H_2 reacts with H_2 to form H_3^+ that is accelerated and breaks up to form H_2^+ or $H^+ + H$ or hits the wall. At the higher E/N the accelerated H_2^+ can break up to form $H^+ + H$. The accelerated H^+ can charge transfer with H_2 to produce fast H atoms that excite H_α. The fast H_2^+ can also charge transfer with H_2 to produce fast H_2 followed by excitation of some H_α. At the low E/N of 350 Td, the H_3^+ mostly breaks up to form H^+ and two H atoms. The accelerated H^+ can undergo charge transfer to form fast H. Our model says that the H_α is excited by fast H and, at high E/N, by fast H_2. We next summarize the cross-section data applicable for each reaction and for elastic and inelastic scatterings.

III. COLLISION CROSS SECTIONS FOR MODEL

In this section, we show graphs and present brief discussions of the cross sections for collisions of various ions and

neutral species with H_2 and with relevant surfaces used in our model. More detailed discussions of the sources of our integral cross sections and some information on the associated differential cross sections are available [40]. Our present cross-section set is significantly different than those of Phelps [42], Heim and Störi [15], Šimko *et al.* [16], Tabata and Shirai [43], and Bogaerts and Gijbels [44] that were developed to describe discharges in drift tubes and glow discharges. Our set also differs significantly from those of Bhardwaj and Singhal [45], Rego *et al.* [46], Bisikalo and Shematovich [47], and Miller *et al.* [48] who have proposed sets for analysis of the role of hydrogen ion and atom excitation of hydrogen emission in the atmospheres of the outer planets. Our cross-section set differs considerably from the experimental set of Okuno [49]. Inelastic cross sections for collisions among hydrogen ions and neutrals of interest in fusion plasmas [50], with emphasis on the theory for various vibrationally excited states, have recently been reviewed in an unpublished report by Janev *et al.* [51]

Some of the graphs presented here are from analytical fits to tabulations in Ref. [42]. Phelps [40,42] and Bogaerts and Gijbels [44] discussed the then available data sources, so that we will emphasize the new references. We have not reexamined the near thermal cross sections discussed in Ref. [42]. All cross sections presented are in m^2 and the kinetic energies cited are laboratory energies in eV. In this paper we do not discuss electron-H_2 cross sections but make use of experimental and empirical Townsend-type excitation and ionization coefficients [52,53] (see Appendix A). Collisions of energetic species with electrons, ions, excited states, and dissociation products are negligible at the low-current densities of the drift tube and low-current density, cathode fall experiments to which our model applies. Negative ions are assumed to undergo collisional detachment very quickly for conditions of interest to us and are not included in the model [16,42].

The cross sections presented here contain no explicit angular scattering information because our model assumes that the collision products continue to move in their original axial direction. Thus, the multibeam model developed in Sec. IV assumes that at the energies of importance the differential cross sections are sharply peaked in the forward direction [40]. The tendency for beamlike behavior is enhanced by the rapid acceleration of the ions in the strong electric fields and the persistence of velocity in heavy-particle collisions. Consistent with this assumption, highly anisotropic ion energy distributions in the direction of acceleration by the electric field are obtained by Bretagne *et al.* [20] in spite of using what appear to be unrealistically broad differential cross sections for ion scattering [40].

We assume that the target H_2 is in the ground vibrational state. This condition is expected to be satisfied at the very-low electrical power input for the drift-tube experiments by our group [1–4]. The internal energy of newly formed [54,55] H_3^+ and the increase in internal energy of H_2^+ and H_3^+ drifting in an electric field, such as found [56] for N_2^+ in He, have not been included in our model.

In the sections that follow, we use the identifier 1 for H^+, 2 for H_2^+, 3 for H_3^+, A for H atoms, and M for fast H_2. All of these species are represented by beams approaching the cathode. The symbol R is used for H atoms leaving the cathode. The products of collisional reactions are further identified by a prefix *f* for fast, i.e., the product has a significant fraction of the initial projectile velocity, and *s* for slow, i.e., the product is effectively at rest in the laboratory frame. For example, *f*1 indicated that the product H^+ continues moving in the direction of the projectile with a non-negligible kinetic energy dependent on the reaction.

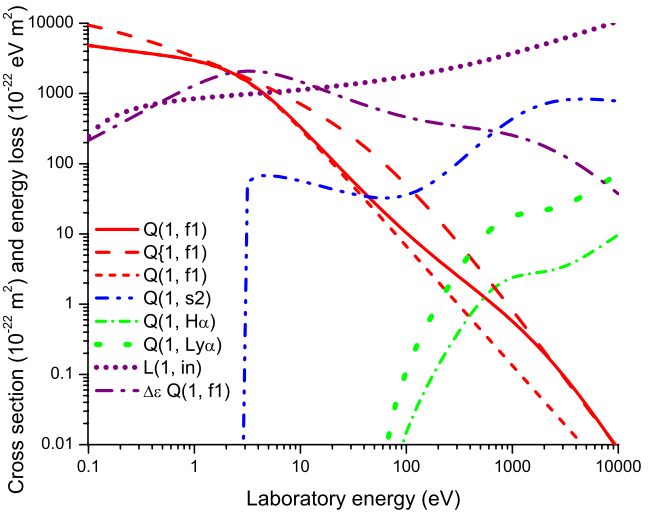

FIG. 2. (Color online) Cross sections for collisions of H^+ with H_2. The curves show the analytic approximations used in the model. The classes of cross sections and their colors are momentum transfer, red; energy loss functions, purple; reaction, blue; and excitation, green. For clarity, the subscript and superscripts of Q in the text become the first and second symbols in parentheses of the $Q(x,y)$. The short and long dashes for $Q(1,f1)$ are from Refs. [42,57], respectively. The solid curve for the total momentum transfer cross section $Q(1,f1)$ is used in our model.

A. Cross sections for $H^+ + H_2$

Our cross-section set for $H^+ + H_2$ collisions is shown in Fig. 2. The momentum transfer or diffusion cross section $Q_1^{f1}(\epsilon)$ for H^+ is indicated by the solid curve. As discussed in Sec. IV A, this collision produces H^+ that has lost $2mM/(m+M)^2 = 4/9$ of its initial energy. An important difference from the earlier cross-section set [42] is the adoption of the sum of the elastic and inelastic cross sections for momentum transfer of Krstić and Schultz [57] for energies below about ~100 eV. At above 100 eV, we make a transition to the values derived by Phelps [42] from measurements of the total differential cross section of Stebbings and coworkers [58].

The cross sections of Fig. 2 differ rather importantly from those of Šimko *et al.* [16] because of their assumption of differential scattering cross sections for rotational and vibrational excitation processes that are very much broader in angle than those calculated by Krstić and Schultz [57].

Another important change from our earlier recommendation [42] is the adoption of a cross section $Q_1^{H_\alpha}$ for the excitation of H_α by H^+ at energies below ~1 keV that is based on scaling the measurements of Lyman α excitation by Van

Zyl *et al.* [59] to fit the measurements of H_α by Williams *et al.* [60] at above 1.5 keV. The resultant cross section is consistent with the energy dependence, but not the magnitude, found for H_α excitation by Hess [61]. This change effectively raises the threshold for H_α excitation from our previous recommendation [42] and reduces the rate of excitation by H^+ significantly at the lower E/N in Ref. [2].

Our charge transfer cross section $Q_1^s 2$ for producing slow H_2^+ is unchanged from Ref. [42]. We neglect vibrational excitation in these collisions, so that the energy of the fast H atom produced is that of the incident H^+.

Inelastic collisions appear in our equation for the distribution in ion energy and position through their contribution to the momentum transfer cross section and through the continuous energy loss function [62] $L_1^{in}(\epsilon)$. The loss function is the sum of the products of energy loss and excitation or ionization cross section. At energies above 1 keV, our $L_1^{in}(\epsilon)$ increases so as to agree with theoretical "stopping power" models and experiments [42]. In Fig. 2, $L_1^{in}(\epsilon)$ is shown as a purple dotted line. For comparison, we also show as a dashed purple chain line the product of the energy loss to target recoil and the momentum transfer cross section. We see that the inelastic energy loss $L_1^{in}(\epsilon)$ exceeds the recoil energy loss at energies above about 20 eV. This behavior is typical of all our cross-section sets, except for $H_2^+ + H_2$.

The ion mobility and mass spectrometer experiments of Albritton *et al.* [17] and of Miller *et al.* [18] yield the three-body rate coefficient for conversion of H^+ ions to H_3^+ ions for $E/N \sim 20$ Td. We adopt the assumption of Johnsen *et al.* [24] that the three-body rate coefficient decreases with the square root of the average H^+ energy. This leads to a rate coefficient that decreases with increasing E/N and our estimate that less than 1% of the H^+ ions are converted to H_3^+ at all E/N and pressures of the drift-tube experiments in Ref. [2]. Contrary to Dexter *et al.* [14], we neglect this process.

B. H^+ + surface → reflected fast H

The fast H^+ is assumed to be reflected from our thin-film gold-palladium (AuPd) cathode as fast H with an energy and angle integrated probability of escape $RAu_1^A(\epsilon)$ given by scaling in energy an empirical fit to calculations for tungsten by Eckstein and Biersack [63], using a theoretically predicted energy scaling factor [64] of 1.08. Thus, we use

$$RAu_1^A(\epsilon) = 0.95[1 + \{0.4/(1 + 1.08\epsilon)\}^2]^{-1}[1 + (1.08\epsilon/7)]^{-0.15}/[1 + (1.08\epsilon/30\,000)]^{1.35}, \quad (1)$$

where the subscript 1 refers to H^+ and the superscript A refers to the product fast H atom. For our graphite cathode, we use a fit to calculations by Aratari and Eckstein [65] for amorphous carbon of

$$Rgr_1^A(\epsilon) = 0.8[1 + \{1.4/(1 + \epsilon)\}^4]^{-1}[1 + (\epsilon/5)]^{-0.35}[1 + (\epsilon/3000)]^{-1.15}. \quad (2)$$

We assume that the reflected H atoms are distributed uniformly in energy, so that their mean energy is 1/2 of the initial kinetic energy. The uniform energy distribution is approximate agreement with a recent experiment and calculation [66]. We have not explored the effects of the nonuniform distributions of reflected atom energies calculated to become more peaked near the maximum available energy as the energy of the incident ion decreases [64,65].

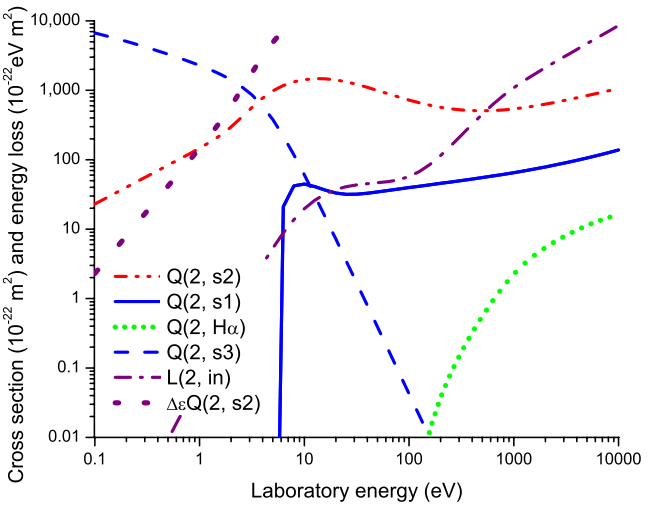

FIG. 3. (Color online) Cross sections for collisions of H_2^+ with H_2. The $Q(x,y)$ notation is the same as for Fig. 2.

We use the very nearly cosine distribution per unit solid angle of reflected atoms measured and calculated for a randomly incident beam [64] that is assumed to apply for an arbitrary angular distribution of incident ions and randomly oriented surface crystallites [67] (see Sec. V A). Reflection as a positive or negative ion is neglected [68].

C. Cross sections for $H_2^+ + H_2$

The cross-section set for $H_2^+ + H_2$ collisions is shown in Fig. 3. These cross sections are assumed to be appropriate to H_2^+ in its ground vibrational state. Thus, we neglect any vibrational excitation acquired by the H_2^+ as it drifts through the room temperature H_2. Note that symmetric charge transfer Q_2^{s2} is the only aspect of elastic scattering included in our model of $H_2^+ + H_2$ collisions. This is because the polarization or Langevin scattering at low energies appears to result in H_3^+ formation rather than elastic scattering [42].

Our previously [42] recommended cross section $Q_2^{H_\alpha}$ for H_α excitation by H_2^+ has been lowered drastically at energies below about 1 keV. As for H^+, the energy dependence now follows the energy dependence (not magnitude) measured by Hess [61]. The high energy portion is unchanged.

The cross section Q_2^{s3} for the formation of slow H_3^+ by proton transfer in $H_2^+ + H_2$ collisions from Table I in Ref. [42] is unchanged. The potentially significant internal energy [69] of the product H_3^+ is not tracked in the present model. Of particular interest for our model is the rapid drop in the H_3^+ formation cross section at H_2^+ laboratory energies above about 10 eV.

The symmetric charge transfer process Q_2^{s2} is assumed to produce a zero energy H_2^+ ion and a fast H_2 molecule with the velocity of the incident ion. We neglect any vibrational excitation of the projectile, target, and products [69,70]; i.e., this assumed to be an elastic collision. Note that this cross

section does not increase with decreasing energy at low energies as recommended in Ref. [51] (see Ref. [71]).

The total dissociative charge transfer cross section of Table IV in Ref. [42] has been divided into equal parts, i.e., the same cross section Q_2^{s1} for the production of slow H^+ as the cross section Q_2^{f1} for fast H^+ because we know of no separate cross-section data. Our H_α production results seem insensitive to this division. In the first case, the products H^+ and H are assumed to be produced by target dissociation and to have negligible laboratory energy. The neutralized projectile H_2 is assumed to continue with negligible energy loss and deflection. Because of their low energy, we neglect the H atoms produced in these collisions. The second case is treated as projectile dissociation, i.e., the H^+ and H are assumed to retain their initial velocities and the energy required for dissociation is neglected.

The continuous energy loss function $L_2^{in}(\epsilon)$ for H_2^+ collisions with H_2 is obtained by summing the products of the energy loss and our previous recommended cross sections for the various inelastic collisions [42]. This function is shown in Fig. 3 as a dashed-dotted curve. In spite of considerable uncertainty, it is seen to be negligible compared to the energy loss in elastic collisions shown by the widely spaced dotted curve. This is because elastic symmetric charge transfer collisions of H_2^+ with H_2 occur with a large cross section and result in thermal H_2^+ and fast H_2.

D. H_2^++surface→2 fast H

The collision of fast H_2^+ with the surface is modeled [65] as that of a H^+ atom and a H atom with half the energy of the incident H_2^+. The H atom and H^+ ion are each reflected as a H atom, with a probability given by Eq. (1) for a AuPd surface or Eq. (2) for a graphite surface, and spread uniformly over the available energy. The assumed reflection appears to apply to within the large scatter of experimental data [65] for H_2^+ on Ni. We assume diffuse backscattering of the H atoms, i.e., the same angular distribution as for H from H^+. The finding by Babkina *et al.* [66] that the contribution of H_2^+ to the reflected fast H flux is negligible compared to that contributed by H^+ suggests that this process will not be important in our model.

E. Cross sections for H_3^++H_2

Our cross-section set for H_3^++H_2 collisions shown in Fig. 4 is very different than that recommended in Ref. [42]. These cross sections are also significantly different than those of Heim and Störi [15], who argued for negligible breakup of H_3^+ in collisions with H_2 in their cathode sheath discharge. We have attempted to assemble cross sections appropriate to H_3^+ ions that are thermally relaxed, e.g., we assume that the ~1.5 eV of internal energy resulting from the H_2^++H_2 →H_3^{+*}+H reaction is rapidly dissipated in collisions with ambient-temperature H_2 [54]. We have no information as to the vibrational "temperature" of the drifting H_3^+ in our apparatus or of reaction cross sections versus energy for vibrationally excited H_3^+.

The cross section for excitation of H_α, $Q_3^{H_\alpha}$, shown in Fig. 4, is a fit to the data of Williams *et al.* [60] at $\epsilon > 3$ keV and

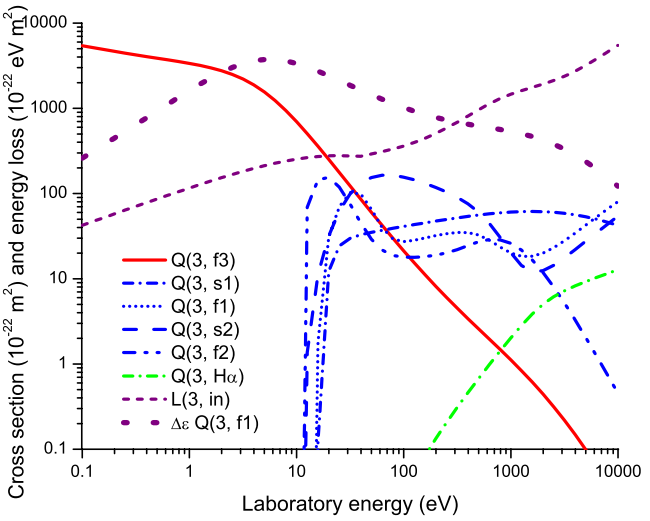

FIG. 4. (Color online) Cross sections for collisions of H_3^+ with H_2. The $Q(x,y)$ notation is the same as for Fig. 2.

is assumed to decrease with energy below 1 keV in the same manner [59,61] as for H^+ and H_2^+ excitation of H_α. We include the energy loss from this excitation in our continuous energy loss approximation when calculating H_3^+ kinetics. From extrapolation of the data of Williams *et al.* [60] to our generally lower energies, we estimate ~10% of the excitation to be dissociative and produce isotropically directed H(n=3) with kinetic energies of a few eV. The other ~90% is assumed to produce H(n=3) with the projectile velocity.

Collision induced dissociation of the H_3^+ leading to fast H^+, fast H_2, and slow H_2 is shown as Q_3^{f1} in Fig. 4. For laboratory energies from 7.3 to 200 eV this cross section is that obtained by Peko and Champion [72]. At higher energies, our fit passes through the results of Williams and Dunbar [73]. This fit agrees with that of Janev *et al.* [51] for energies below 20 eV but is somewhat smaller and has more structure at higher energies. The threshold for this reaction [72] in laboratory frame is 7.3 eV. The velocities of the H^+ and H_2 are assumed to be that of the projectile, e.g., the kinetic energy of the H^+ is 1/3 of that of the incident ion.

Collision induced dissociation of H_3^+ leading to fast H_2^+, fast H, and slow H_2 is shown as Q_3^{f2} in Fig. 4. This cross section is that obtained by Peko and Champion [72] for product ions with an axial energy of approximately 2/3 of the energy of the incident ion. Our fit passes though the fast H_2^+ results of McClure [23]. Our derived cross section for the production of fast H_2^+ is much larger than that of Šimko *et al.* [16] below about 100 eV.

Charge transfer producing slow H_2^+ and fast H_3 followed by dissociation of the fast H_3 into H and H_2, each with the velocity of the projectile, is shown as Q_3^{s2} in Fig. 4 from Peko and Champion [72]. The cross section has a threshold of 11 eV in the laboratory. Our simplified model neglects the vibrational and rotational levels of the products. Our cross section is very different than that of Šimko *et al.* [16,74], especially at energies below 100 eV.

Proton transfer from H_3^+ followed by H_3^+ dissociation to produce slow H^+, slow H_2, and fast H_2, Q_3^{s2}, is reaction (4b) of Peko and Champion [72]. It is shown for H_3^+ laboratory

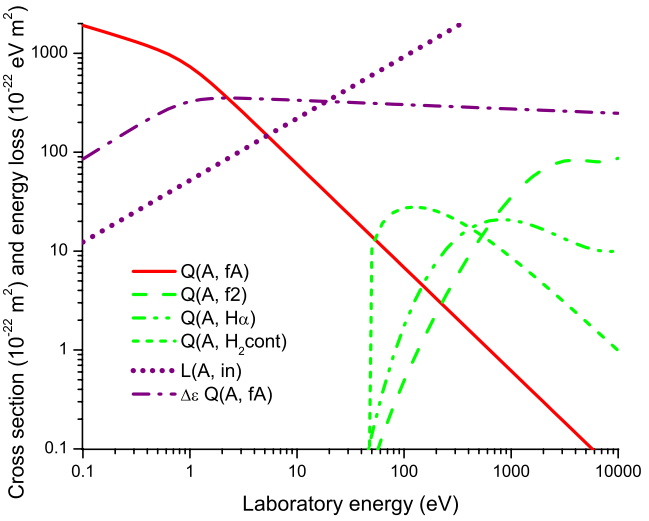

FIG. 5. (Color online) Cross sections for collisions of H atoms with H_2. The $Q(x,y)$ notation is the same as for Fig. 2.

energies from the threshold of 15.5 eV (LAB) to 450 eV. At higher energies we use the data of Huber *et al.* [75], who measured the slow H_2^+ formation cross section at energies from 300 to 1250 eV. Our cross section is very different than that of Šimko *et al.* [16], especially at energies below 40 eV. The fast H_2 is assumed to have the velocity of the projectile or 2/3 of its energy.

The continuous energy loss function $L_3^{in}(\epsilon)$ for H_3^+ in H_2 is obtained by summing the products of the excitation thresholds for the various inelastic collisions and their cross sections. At energies above about 20 eV, this energy loss function is obtained by doubling the products of energy loss and cross section for electronic excitation and ionization shown in Ref. [42] to allow for unmeasured excitation. Below about 10 eV, this energy loss is based on the estimate discussed in Sec. I for H^+ ions. At H_3^+ energies approaching 10 keV we have increased $L_3^{in}(\epsilon)$ so that it approaches $3\times L_1^{in}(\epsilon/\sqrt{3})$, as suggested by measurements in solids at energies above 30 keV [76]. The predicted emission from our model is relatively insensitive to the accuracy of this energy loss function because of the larger elastic recoil energy loss at the low energies and low E/N at which H_3^+ reactions are important.

F. H_3^++surface→3 fast H

We assume that on collision with the cathode the fast H_3^+ dissociates into three fast H^+ ions, each with an available energy equals 1/3 of that of the incident H_3^+ [64,65]. The ions are neutralized and the energy of each of the reflected atoms is spread uniformly over the available energy with the same probability as a H^+ ion discussed above. These values are typical of measurements for H_3^+ on Ni when scaled for target mass [65] (see Sec. IV). We assume the same angular distribution of backscattered atoms as for H from H^+.

G. Cross sections for H+H_2

Our cross-section set for H+H_2 collisions is shown in Fig. 5. Most of the cross sections for collisions of H with H_2 are fits to the data of Fig. 8 and Table VIII in Ref. [42]. The accuracy of the analytical fits is ±10%. Because of their small cross sections, we neglect various ionization and negative ion formation processes [42].

Our fit to the cross section for the excitation of the H_α line in the absence of collisional quenching, electric field level mixing, and absorption of the Lyman β line as measured by Van Zyl *et al.* [77] is treated as the reference cross section for our model. Because this energy loss is included in our energy loss function for H atoms, this loss does not appear separately in our multibeam calculation of H atom kinetics. An important aspect of the excitation of H_α by H atoms is the observation [60] of a division of the excitation into projectile excitation of H atoms with the incident atom velocity and target excitation of H_2 followed by dissociation to produce H_α with less than about 10 eV. The measured fraction of the H+H_2 collisions that produce target excitation varies from ≈10% at 2 keV to ≈40% at 15 keV [60]. We adopt the value of 10%.

We have found no cross-section data on the excitation of the near-uv bands of H_2 by H atoms, although its production by "kanal" rays, i.e., ions, atoms, and molecules passing through a hole in the cathode, has been observed [78]. Similarly, we have found no information on the excitation of the far-uv bands of H_2 by H atoms. Our choice of excitation cross section to fit the observed emission of the $H_2(a^3\Sigma)$ continuum is shown in Fig. 5 as Q_A^{uv}. Note the relatively large cross section that peaks at relatively low energies compared to that for H_α excitation in H+H_2 collisions. This behavior suggests favorable potential curve crossings for the excited H_3 molecule.

Our model utilizes the diffusion (momentum transfer) cross section $Q_A(fA)$ shown by the solid curve in Fig. 5 to calculate the energy loss in elastic collisions. From Eq. (7) of Sec. IV A, elastic scattering of H atoms results in a fractional energy loss of 4/9 of the laboratory energy of the incident H atom, where the $(1-\cos\theta)$ factor is included in the diffusion cross section. Krstić and Schultz [57] found that vibrational excitation makes a very significant contribution to the diffusion cross section (solid) at energies above ~30 eV. As discussed for H^+ in Sec. III A, at the higher energies we make a gradual transition to the recommendation of Phelps [42] shown by the solid curve.

The continuous energy loss function L_A^{in} representing the effects of inelastic collisions for H in H_2 is obtained by summing the products of the energy loss, assumed to be the excitation thresholds, for the various inelastic collisions times their cross sections. This function includes the contribution of the far- and near-uv excitation processes. The resultant energy loss function oscillates ±20% about our analytic approximation to L_A^{in} shown.

The collisional quenching of the H_α state by H_2 has been measured by a number of authors with widely divergent results [79–84]. Complications in analyzing such data include (a) uncertainties in the relative excitation cross sections for the various fine structure levels and (b) the very significant electric field mixing [85] of the fine structure levels of the $n=3$ and higher levels at our electric field strengths of 25–450 V/cm. We will treat the effective quenching rate coefficient as an unknown constant rate coefficient to be determined from our experiments [2].

H. Reflection of fast H as fast H

We use the same backscattering function as for H^+. The uniform energy distribution is in approximate agreement with a recent experiment and application of particle reflection codes [65,66]. We assume that the reflected H atoms have the same angular distribution of velocities relative to the normal to the cathode surface as for H from incident H^+ [64]. Because we neglect the angular scattering in collisions of H atoms with H_2, velocities transverse to the electric field arise from diffuse backscattering at the cathode. This assumption also leads to an effective increase in the collisional attenuation of the H atom flux normal to the cathode (see Sec. IV).

I. Loss of fast H at wall

In this section we estimate the effects of the loss of fast H atoms at the side wall of the drift tube used in our experiments [2–4]. We assume that the fast atoms are effectively destroyed by striking this quartz wall [86], although we have found no directly relevant experiment or theory for quartz. In this estimate, gas phase collisions are assumed infrequent. For a diffuse source at the center of the cathode, the rate of H_α excitation $S(z,R,\epsilon)$ by the H atom flux passing through a disk of thickness $\triangle z$ and radius R located at a distance z from the cathode is

$$\begin{aligned} S(z,R,\epsilon) &= \int_{x=z}^{x=z+\triangle z} \int_{r=0}^{r=R} \Gamma_0(\epsilon) \\ &\quad \times (1/\rho)^2(\cos\,\theta/\pi) Q_A^{\mathrm{H}\alpha}(\epsilon) N 2\pi r dr dx \\ &= \Gamma_0(\epsilon) Q_A^{\mathrm{H}\alpha}(\epsilon) N \triangle z\{1-(z/R)[1+(z/R)^2]^{-1/2}\} \\ &\approx \Gamma_0(\epsilon) Q_A^{\mathrm{H}\alpha}(\epsilon) N \triangle z \exp[-1.2z/R] \quad \text{for } z/R < 2. \end{aligned} \tag{3}$$

Here $\Gamma_0(\epsilon)$ is the rate of H atom emission from the center of the cathode, $\rho=(x^2+r^2)^{1/2}$, $\cos\,\theta/\pi$ is the assumed normalized angular distribution of H atoms per unit solid angle as a function of the polar angle θ, and $Q_A^{\mathrm{H}\alpha}(\epsilon)N$ is the rate of production of H_α atoms per unit distance in the electric field direction. The angular distribution of the H atoms is discussed further in Sec. V.

A similar dependence on z is obtained for a diffuse source located at outer edge of the cathode at the wall. We will take advantage of the approximate exponential behavior and approximate the wall loss as a volume loss process for the H atoms. Thus, the wall loss can be simulated approximately by a flux attenuation coefficient of $1.2/R$ for our $d/R<2$. Because of possible fast atom reflection, this is an upper limit to the loss of H atoms leaving the cathode [2]. We have not applied this approximate wall loss to the fast H atoms or ions moving toward the cathode because of their production nearer the cathode. However, our later assumption of a cosine law for the angular distribution of excited H atoms approaching the cathode suggests that wall loses for these atoms should be reconsidered.

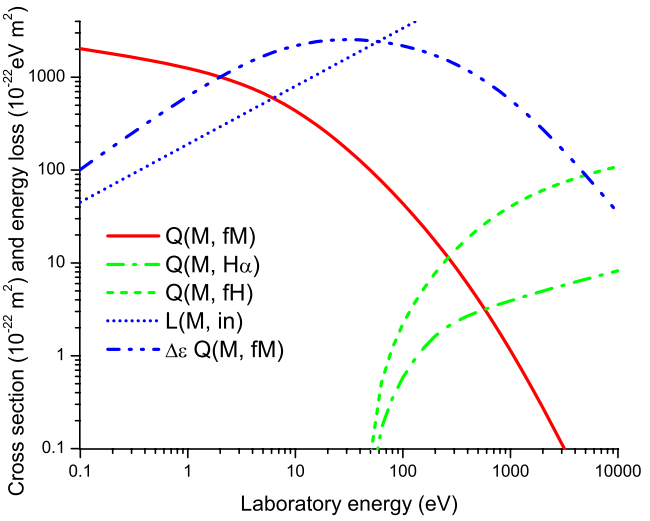

FIG. 6. (Color online) Cross sections for collisions of H_2 with H_2. The $Q(x,y)$ notation is the same as for Fig. 2.

J. Cross sections for H_2+H_2

Our limited cross-section set for H_2+H_2 collisions is shown in Fig. 6. The momentum transfer cross section for H_2 molecules in their ground state with H_2 is a fit to the data in Ref. [42]. As will be discussed in Sec. IV A, this process results in a fractional energy loss of 1/2 the initial laboratory energy of the H_2 per momentum transfer collision. We neglect the contribution of rotational excitation and vibrational excitation to momentum transfer scattering Q_M^{fM} because we have no relevant cross-section data. Our model neglects various positive and negative ion formation processes involving fast H_2 molecules [42].

The continuous energy loss function L_M^{in} for H_2 in H_2 is obtained by summing the products of the excitation thresholds and their cross sections from Ref. [42]. Because of the large uncertainties and multiple small fluctuations in this function, we have fit the sum only to $\pm 20\%$ at energies above 20 eV and $\pm 40\%$ for energies from 2 to 20 eV. This fitted energy loss does not include the unknown Lyman α excitation.

The only experimental cross-section data we have found for the excitation of H_α by H_2 is for 10 keV and higher [87]. From the comparison with experiment [2], we conclude that the extrapolation of the high energy data to threshold recommended in Ref. [42] is much too large. Our suggested cross section $Q_M^{\mathrm{H}_\alpha}$ gives a noticeable contribution to the Doppler profile of Sec. V. We assume that this dissociative excitation produces a H($n=3$) atom and a H($n=1$) atom with each having half the projectile energy and no deflection. One reason for including this excitation process is the apparent importance in the excitation by fast N_2 in high E/N experiments with N_2 [88].

The destruction of fast H_2 in collisions with H_2 is assumed to have the cross section given in Ref. [42] for energies above 2.5 keV. These dissociation collisions are assumed to result in two H atoms, each with the velocity of the incident H_2 molecule. At lower energies, we have lowered the extrapolated cross section from Ref. [42] to approach the

new cross section for H(n=3) excitation and to improve the fit of the model to the H_α Doppler profile discussed in Sec. V.

K. Reflection of fast H_2 as two H atoms

We use the same backscattering function as for H_2^+. We assume that the reflected H atoms have the same angular distribution as for H from H^+. We assume a uniform distribution of H atom energies from zero to half the incident H_2^+ energy.

IV. CALCULATION OF ION AND NEUTRAL PARTICLE FLUXES

In this section we outline the procedure used to calculate the spatial and energy distributions of the ions and neutral species. The model results are then used to obtain the spatial distribution of H_α emission for comparison with data [2]. We also compare our model results for the ion-flux energy distribution at the cathode with published experiments and models [19,20,89]. In Sec. V, we will use these results to calculate H_α Doppler line profiles for comparison with experiment [3].

A. Flux equations

The equations governing the flow of charged and fast neutral particles are illustrated by writing out the multibeam equations for H^+ ions moving toward the cathode. Our derivation follows that for electrons in Ref. [90]. The corresponding equations for H_2^+(toward), H_3^+(toward), H(toward), H(n=3)(toward), H_2, H(away), and H(n=3)(away) are formulated using the cross sections given in Sec. III.

We begin by writing the Boltzmann equation [90] in the one-dimensional laboratory frame for the velocity distribution $f_1(z,\theta,v)$ for the H^+ ion, labeled 1, at position z with a speed v and a velocity polar angle θ in the form

$$\partial f_1(z,\theta,v)/\partial t + \nabla_z v_z f_1(z,\theta,v) + a\nabla_v f_1(z,\theta,v) = -\sum_k 2\pi v N f_1(z,\theta,v)\int_{\psi=0}^{\pi} I_k(v,\psi)\sin\psi d\psi + \sum_k 2\pi v \int_{\theta'=0}^{\pi} I_k(v',\psi) N f_1(z,\theta',v') \times \sin\theta'(v'/v)^2(dv'/dv)d\theta', \quad (4)$$

where the first term is zero in our steady-state model. The second term is the flow in coordinate space. The third term is the flow in velocity space, where $a=eE/m_i$ is the acceleration, e is the electron charge, E is the spatially uniform electric field, and m_i is the ion mass. The first term on the right-hand side is the sum over the rates of loss of species i to a lower velocity resulting from elastic or inelastic collisions or to another species by reactive collisions. The second term is the sum of the rates of gain from higher velocities by elastic and inelastic collisions and gain by reactions. $I_k(v,\theta)$ is the differential cross section for the $k\prime$th elastic or inelastic process or ion-molecule reaction, ψ is the scattering angle in center of mass, and the summations are over all collision processes.

We next take the first moment in the field direction and make the substitution [90]

$$v_z f_i(z,v_z) = J_i(z,v_z)\delta(v-v_z)\delta(\theta)/(2\pi v^2\sin\theta), \quad (5)$$

where $J_i(z,v_z)$ is the flux velocity distribution, v_z is the field directed component of velocity, and $\delta(x)$ is the Dirac delta function at x=0. A change in variable using $m_i v_z^2/2=\epsilon_z$ gives

$$\partial j_i(z,\epsilon_z)/\partial z + eE\,\partial j_i(z,\epsilon_z)/\partial\epsilon_z = -\sum_i Q_k(\epsilon_z)N j_i(z,\epsilon_z) + \sum_i \int_{\epsilon_z=0}^{eEz} Q_k(\epsilon_z')N j_i(z,\epsilon_z')d\epsilon_z'/\epsilon_z', \quad (6)$$

where $j_i(z,\epsilon_z)$ is the flux energy distribution. This equation says that the ions move toward the cathode at constant total energy between collisions. For the neutral atoms and molecules the electric field term representing acceleration is zero and these particles move toward or away from the cathode at constant kinetic energy between collisions. We assume that there is a negligible flux of ions and fast atoms leaving the anode [91].

We now consider the contribution of elastic collisions to the summations in Eq. (6). Elastic collisions reduce the projectile ion or neutral energy by the recoil energy given to the target H_2 molecule. This energy is given by [92,93]

$$\Delta\epsilon = [2mM/(m+M)^2]\epsilon(1-\cos\phi), \quad (7)$$

where m and M are the masses of the projectile and target and ϕ is the scattering angle in the center of mass [93]. We note that the angular dependence is that which defines the diffusion or momentum transfer cross section and so use this cross section in our model. In the case of inelastic collisions, we use the momentum transfer weighted cross section for the recoil portion of the energy loss. The change in internal energy of the colliding species is included in the model by use of the "continuous energy loss" approximation [62], i.e., the sum of the excitation energies times the corresponding angular integrated or "total" excitation cross section. The error introduced by this approximation is reduced by the small magnitude of the excitation energies compared to the typical projectile energy, as for rotational and vibrational excitation, and by the slow increase in most heavy-particle cross sections above threshold.

The numerical scheme for calculating the spatial and energy distributions of the fluxes utilizes the multibeam approximation [15,94,95] to describe the fluxes of H^+, H_2^+, H_3^+, H and H_2 moving toward the cathode, and H moving away from the cathode. The kinetic energy space is divided into a number of equal energy intervals each represented by a beam equation similar to that of Eq. (5). We use a finite difference technique to write coupled algebraic equations [15], derived from equations such as Eq. (6), for the distribution in space of our six heavy-particle species. Collisions result in flow only downward in total energy (kinetic plus potential). Therefore, we start at the highest total energy and then consider the next lower total energy. Our simplified col-

lision and transport model allows one to separate the equations for the ions, atoms, and molecules moving toward the cathode from the equations for the fast atoms moving away from the cathode.

For most of the calculations, we have used a fluid model to calculate the electron behavior assuming the empirical spatially independent ionization and excitation coefficients from Appendix A. The ionization coefficient calculated for electrons using the two-term Boltzmann equation works well for $E/N \leq 350$ Td, but data discussed in Appendix A show that it is in error by a factor of about 2.5 for $E/N=10$ kTd. We use an empirical electron ionization coefficient determined initially from current-growth experiments [4] and fine tuned to fit the emission data in Ref. [2]. Empirically, application of our multibeam model to electrons is found to work satisfactorily at E/N of 350 Td and 10 kTd [4], but we have not investigated its general usefulness.

For the calculations reported in this paper, we have assumed that the lifetimes of the H($n=3$) state ($\sim 1\times 10^{-8}$ s from Refs. [85,96]) and the $H_2(a^3\Sigma)$ state (1×10^{-8} s from Ref. [97]) are short enough so that the excited atoms and molecules do not move significantly before radiation (see Appendix B for a more detailed discussion). The scheme for determining the effective quenching coefficient for the excited H($n=3$) atoms is described in Ref. [2]. The calculated results for a very high E/N of 10 kTd and for one of our lower E/N of 350 Td are discussed next. More extensive comparisons of our predictions with experiment are given in Ref. [2].

B. 10 kTd model results

Figure 7(a) shows calculated steady-state fluxes of H^+, H_2^+, H_3^+, fast H atoms, and fast H_2 as a function of distance from the cathode for E/N of 10 kTd and a hydrogen pressure of 0.14 Torr. These fluxes are normalized to unit electron flux at the anode. The small ($\sim 3\%$) departure of the sum of the fluxes of charged particles in Fig. 7 from unity at the cathode provides a measure of the accuracy of our numerical calculation. The reaction rate balances for production and loss of each of the ionic species in Fig. 1(a) are also indicative of reasonable calculation accuracy. The neutral particle rate balances are more difficult to interpret because of the build up of inactive H atoms and H_2 molecules in the lowest energy bin. We note the delay in build up of the ion fluxes moving away from the anode in the order indicated in the reaction sequence of Fig. 1, e.g., the H_2^+ is followed by H_3^+ and then H^+. The H atom flux moving toward the cathode quickly exceeds the H^+ flux by a large factor. The near constancy of ratios of the three ion-flux curves toward the cathode is indicative of a quasiequilibrium maintained by reactions among the three ions.

Particularly relevant for this paper is the comparison of calculated and measured H_α emission versus position in Fig. 7(b) for $E/N=10$ kTd. The measured values are those published in Fig. 2 in Ref. [1] and described in Ref. [2]. The calculated values are obtained by multiplying the normalized fast particle flux densities per unit energy shown in Fig. 7(b) by the respective excitation cross sections from Sec. III and

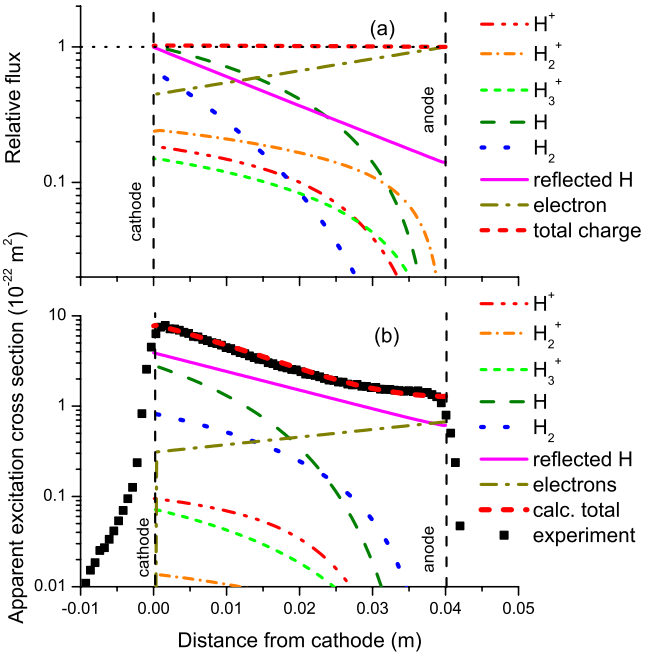

FIG. 7. (Color online) (a) Calculated ion and neutral fluxes for $E/N=10$ kTd and $p=0.15$ Torr versus distance from the cathode for unit total charged particle flux. (b) Calculated (curves) and measured (points) spatial distributions of H_α emission showing calculated contributions of excitation by various species.

the fraction of the H($n=3$) atoms that radiate before being collisionally quenched [2]. The results are integrated over energy to give an effective excitation cross section versus position. Figure 7(b) shows that most of the observed H_α excitation is produced by collision of fast H atoms with H_2. For our conditions this excitation is dominated by fast atoms reflected from the cathode. Excitation by electrons becomes significant near the anode. Further tests of predicted spatially dependent emission are possible when using the transient H_α emission to separate the prompt electron and delayed heavy-particle induced excitation [4].

The numbers on the flow chart in Fig. 1(a) are indicative of the relative importance of various reactions among the ions and fast atoms for $E/N=10$ kTd. These numbers are products of ion or atom flux times cross section times gas density integrated over distance and are normalized to the electron flux at the anode. As such, they are the numbers of reactions of a specific type that occur per electron reaching the anode or per unit charge crossing the gap. For example, the number of 0.019 associated with the arrow from H to H($n=3$) in Fig. 1(a) is obtained by averaging the apparent cross-section curve for excitation by fast H atoms in Fig. 7(b) and multiplying by the H_2 density.

In the case of $E/N=10$ kTd, Fig. 1(a) shows that most of the H_α excitation by heavy particles is via fast H formed from H^+ produced in the breakup of the H_2^+, although a significant amount of H^+ arises from breakup of the H_3^+. According to our fluid model, the flux of electrons grows exponentially with distance from the cathode and leaves behind a cloud of H_2^+ ions that increases with distance from zero at the anode. At the high mean energies of 380, 130, and 440 eV for H^+, H_2^+, and H_3^+, comparable amounts of H_2^+

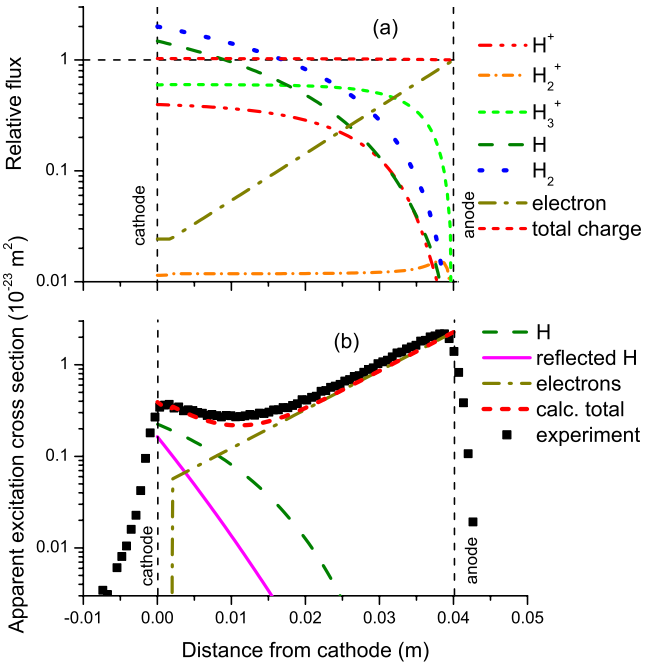

FIG. 8. (Color online) (a) Calculated ion and neutral fluxes versus distance from the cathode for $E/N=350$ Td and $p=0.8$ Torr for unit total charged particle flux. (b) Calculated (curves) and measured (points) spatial distributions of H_α emission showing calculated contributions of excitation by various species.

ions are converted to H_3^+ ions (43%) and to H^+ ions (20%). Some of the H_3^+ breaks up, such that about 40% produce H^+. According to Fig. 1(a), only about 2% of the charged particles crossing the drift space result in H_α at an energy cost of 2 keV per charged particle.

C. 350 Td model results

Figure 8(a) shows calculated fluxes of H^+, H_2^+, H_3^+, fast H atoms, and fast H_2 for E/N of 350 Td and a H_2 pressure of 0.80 Torr. The H_2^+ ions produced by the exponentially increasing electron flux are quickly converted to H_3^+ near the anode because of the large cross section for conversion of H_2^+ to H_3^+ at energies below 10 eV as shown in Fig. 3. Some of the H_3^+ breaks up to produce H^+ and H_2^+. The approach to a quasiequilibrium among the ions is indicated by the near constancy of their relative populations as they approach the cathode. The fluxes of H atoms and H_2 molecules approaching the cathode shown include large contributions of low energy particles that are not reactive. We have not shown the virtually meaningless large total flux of H atoms moving toward the anode and containing a large component at low energies. The small departure (~3%) of the total ion flux from unity is a measure of the accuracy of our numerical calculation.

Figure 8(b) shows calculated and measured spatial distributions of H_α emission for E/N of 350 Td. The calculated values are obtained as described in Sec. IV B. The measured values are from Refs. [2,98]. Figure 8(b) shows that the spatial dependence of emission is dominated by electron impact excitation except near the cathode [99]. This figure shows

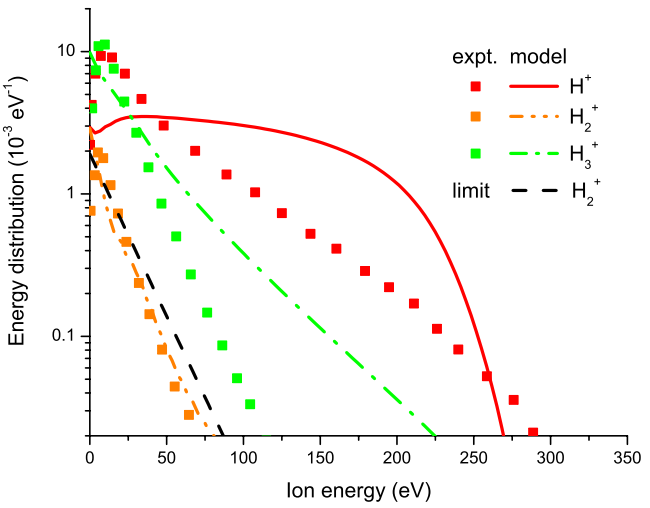

FIG. 9. (Color online) Calculated (curves) and measured (points from Ref. [89]) ion-flux energy distributions for $E/N=1$ kTd, $p=0.49$ Torr, and $d=2$ cm.

that again the heavy-particle excitation is produced by fast H atoms either approaching the cathode or reflected from the cathode. Some of the H_3^+ break up to produce H^+, followed by fast H and finally by $H(n=3)$. This reaction and acceleration chain results in a build up of heavy-particle excitation of H_α emission that varies as a high power of distance from the anode. Similarly, the multiple step reaction sequence followed by H atom induced H_α excitation results in emission near the cathode that increases rapidly with pressure. Examples of this behavior are presented in Ref. [2].

In the case of $E/N=350$ Td, Fig. 1(b) again shows that most of the H_α excitation by heavy particles is via fast H formed by charge transfer from H^+. This H^+ is produced principally by the breakup of H_3^+ rather than the breakup of the H_2^+ as occurs for $E/N=10$ kTd. Note that in spite of the significant fraction of the H atoms produced from H_3^+ breakup, the low energies of the H_3^+ means that these H atoms have low energies and are relatively ineffective in excitation of H_α.

D. Ion energy distributions

Figure 9 show a comparison of our calculated energy distributions for the fluxes of H^+, H_2^+, and H_3^+ at the cathode with the energy dependencies of the measurements of Rao and co-workers [19,89] for $E/N=1$ kTd and various electrode spacings of about 2 cm and an unstated pressure estimated to be about 0.5 Torr. The shape of the calculated flux energy distribution for H_2^+ is in satisfactory agreement with the experiment, but for H^+ and H_3^+ the agreement is poor. The short dashed (black) curve for H_2^+ is a limiting energy dependence calculated under the assumption that only symmetric charge transfer collisions occur [100]. Attempts to improve the fit of our model to the H^+ and H_3^+ data led to unrealistically large momentum transfer cross sections $Q_1^{f1}(\epsilon)$ and $Q_3^{f3}(\epsilon)$ at energies in the 50–1000 eV range [101]. The disagreement between our model and experiment [19] at $E/N=10$ kTd is comparable with that at 1 kTd. We have no

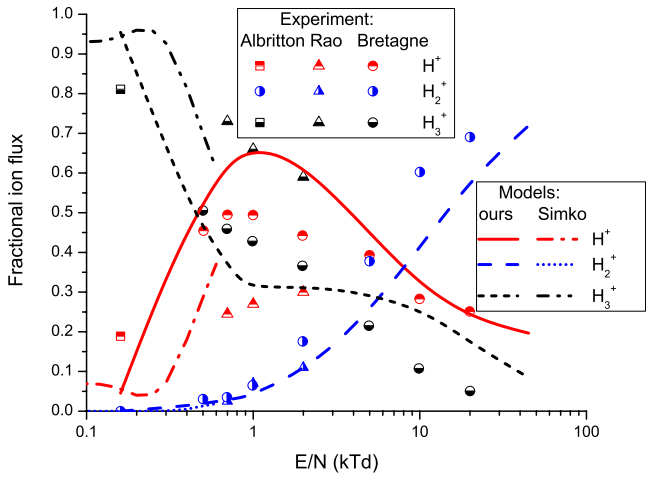

FIG. 10. (Color online) Calculated (curves) and measured (points) fractional ion fluxes at cathode versus E/N. The solid curves are calculated for the highest pressures used in the experiments in Ref. [2], e.g., 0.8 Torr at $E/N=350$ Td to 0.08 Torr at $E/N=45$ kTd. The chain and dotted curves are model results from Ref. [16].

explanation for the discrepancy, but note that Rao *et al.* [100] found that experiment and theory agree well for ions in their parent gas. In these cases, symmetric charge transfer collisions dominate and there is no persistence of ion velocity after a collision so that the ion is more easily focused by the electric fields.

The calculated ion-flux energy distributions are approximately independent of drift-tube length for energies below about half the applied voltage, as observed experimentally [89]. Experiments [89] and our model show that the high energy tails of the H_3^+ energy distributions become much more noticeable at E/N above about 1 kTd, with these high energy tails extending to near the applied voltage. This E/N is approximately that at which our "single-beam" model [102] of ion motion suggested ion "runaway." [42] This transition is not noticeable for H^+ and is not expected for H_2^+ ions.

E. Ion fluxes at cathode

Our calculated energy-integrated fractional ion fluxes at the cathode for H^+, H_2^+, and H_3^+ versus E/N shown by the solid curves are compared with experiment [17,19,89] in Fig. 10. These results show that the dominant ion changes from H_3^+ at low E/N to H^+ at intermediate E/N and to H_2^+ at high E/N. The comparisons of Fig. 10 show that the differences among calculated and measured fractions for H^+ and H_3^+ are comparable with the large scatter in experimental data. The best agreement between our calculations and experiment is for the increasing fraction of H_2^+ as E/N increases. Our model predicts a H^+ fraction decrease from 0.65 to 0.5 and a corresponding increase in the H_3^+ fraction for a pressure decrease from 0.27 to 0.12 Torr at $E/N=1$ kTd and $d=0.04$ m. The effects of pressure are smaller at lower and higher E/N. These changes are to be compared with the observation [19,89] of constant relative ion fluxes for an unspecified change in pressure at fixed E/N.

The calculated ion-flux ratios at the cathode of Šimko *et al.* [16] are indicated by the dashed lines of Fig. 10. These results show the onset of H_3^+ breakup and the buildup of H^+ at about twice the E/N of our model. This trend is expected from the delayed maxima in their H_3^+ breakup cross sections relative to those of Peko and Champion [72] used in our model. Our calculations of Fig. 10 are consistent with the observation by Fletcher and Blevin [103] of a large change in secondary electron yield near $E/N\sim 300$ Td and an increase in the fractional H^+ ion flux with increasing E/N. Our model suggests that fast H atoms approaching the cathode after production by H^+ charge transfer collisions with H_2 may be significant source of secondary electrons [21,104] at the cathode in the experiments of Fletcher and Blevin.

V. MODEL OF DOPPLER PROFILE

In this section we calculate the Doppler profiles expected on the basis of the kinetics model developed in Sec. IV and compare the calculated profile with an experimental profile from Ref. [1]. We discuss the differences in profiles expected when observed parallel and perpendicular to the electric field.

A. Calculation of Doppler profile

The model described in Sec. IV A yields the positions and energies of the ions and fast atoms but gives no information as to the angular distributions of the $H(n=3)$ atoms required for calculations of Doppler profiles. Instead, we adapt angular distributions from models of H^+ and H atom scattering at surfaces [64] so as to fit the present model to the measured H_α Doppler profile. The maximum H_α line splitting [85] caused by the applied electric field (≤ 500 V/cm) is less than 10% of the instrumental resolution in our experiments and will be neglected. The collisional Stark broadening calculated by extrapolating the theory in Ref. [105] to the ion densities ($\leq 10^6$ cm^{-3}) calculated for drift-tube discharges is completely negligible. Similarly, the low gas densities rule out the estimated pressure broadening [106]. For the purposes of this approximate model the electrodes are considered infinite and the discharge is assumed uniform radially. A partial accounting for the finite electrode radius is the loss of fast H atoms to the side walls estimated in Sec. IV. In the following calculation we have neglected the effects of the finite angular aperture of the optical detection system.

Figure 11 shows a schematic of geometry applicable to the calculation of Doppler profiles. Part (a) shows the geometry for viewing through the cathode parallel to the applied electric field, while part (b) shows the geometry for viewing at right angles to electric field. We consider emission from a slab of thickness dz along the axis of the drift tube. We calculate the contribution to the photon flux resulting from emission by a $H(n=3)$ atom in a wavelength interval $d\lambda$ at a wavelength shift from line center, $\Delta\lambda$, while in the slab. We present details only for excitation by fast H atoms because the formulas for excitation of H_2 by fast H^+, H_2^+, H_3^+, and H_2 particles are essentially the same.

In order to consider a range of angular distributions for the fast $H(n=3)$ atoms, we assume the excited H atoms leav-

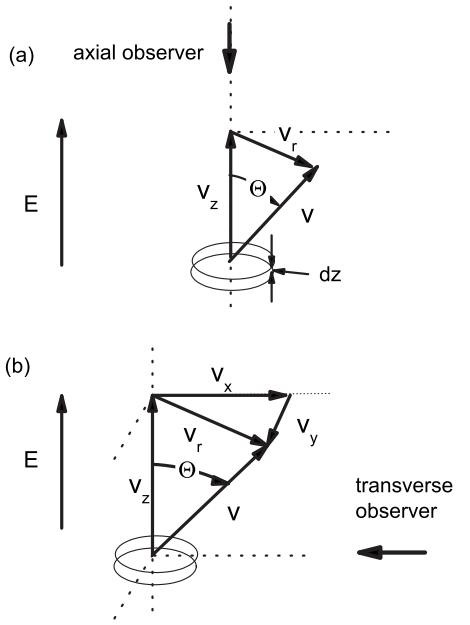

FIG. 11. Schematic of geometry applicable to calculation of Doppler profiles. (a) Geometry for viewing along electric field of discharge. (b) Geometry for viewing at right angles to electric field of discharge.

ing the cathode have a normalized angular distribution per unit solid angle $G(\theta)$ given by

$$G(\theta) = (1+b)\cos\,\theta^{(b+1)}/(2\pi) \tag{8}$$

for $0 \leq \theta \leq \pi/2$ and zero for $\pi/2 \leq \theta \leq \pi$, where $\theta=0$ is directed away from the cathode for reflected H($n=3$) atoms and toward the cathode for H($n=3$) approaching the cathode. Here θ is the polar angle and b is a constant. This distribution changes from a peaked beam along the $\theta=0$ direction for $b \gg 1$, through a cosine distribution for $b=1$, to an almost uniform distribution for $b \ll 1$. The calculated angular distributions for H atoms backscattered from Ni at 450 eV and 4 keV by Eckstein and Verbeek [64] suggest $b=0.6$. In Sec. V B, we will find better fits to experiment using this for H($n=3$) leaving the cathode and a comparably broad angular distribution for the approaching excited atoms. For calculations in which $b \sim 1$, the various $Q_x^y N$ values of the one-dimensional kinetics code were multiplied by the reciprocal of an average of $\cos(\theta)$, i.e., 2, to allow for the increased probability of reaction caused by off-axis motion.

For observations along the axis, we express the velocities in cylindrical geometry as in Fig. 11(a). We calculate the total intensity per unit area of cathode from a slab of thickness dz for a particular v_z corresponding to a wavelength shift $\Delta\lambda$. It is given by an integral over the rate of production of excited atoms per unit volume of excited atoms $j_A(z,\epsilon)Q_A^{\mathrm{H}\alpha}(\epsilon)N$ times the fraction of the H($n=3$) atoms that radiate $A/(A+k_qN)$ times the normalized angular distribution expressed as a function of the velocity components v_z and v_r. Thus, the velocity distribution of the intensity observed parallel to the electric field $I_P(v_z)$ and normalized to the current density is

$$I_P(v_z) = [A/(A+k_qN)](1+b)(M/e)\int_{z=0}^{d}\int_{v_r=0}^{v_r^{\max}} j_A(z,\epsilon)Q_A^{\mathrm{H}\alpha}(\epsilon) \times N v_z^b [v_r/(v_r^2+v_z^2)^{(1+b)/2}]dv_r dz, \tag{9}$$

where A is the radiative transition probability, k_q is the collisional quenching coefficient, and N is the H_2 density. The kinetic energy of the H($n=3$) is $\epsilon = M(v_r^2+v_z^2)/(2e)$, where M is the mass of the H atom and e is the electronic charge. The maximum value of the radial component of the excited atom velocity v_r is $v_r^{\max} = \sqrt{(2eV_0/M - v_z^2)}$, where V_0 is the voltage between the electrodes.

The integral of Eq. (9) is evaluated using normalized fast H atom fluxes $j_A(z,\epsilon)$ from the procedure of Sec. IV under the assumption of a discharge uniformly spread over an infinite electrode surface. The integral is divided by the column density $d \times N$ to yield an average value per atom. Then one converts to the wavelength shift using $v_z = \delta\lambda \times c/\lambda_0$, where λ_0 is the unperturbed wavelength and c is the speed of light. A representative photon flux distribution versus $\delta\lambda$ is shown in Fig. 12. An integral over this distribution $\Delta\lambda$ yields the apparent excitation cross section.

The Doppler profile for excited atoms at position z on the drift-tube axis observed perpendicular (also called transverse) to the electric field is found using rectangular geometry as in Fig. 11(b). For an observer looking perpendicular to the electric field, the normalized velocity distribution of the intensity $I_T(v_z)$ is

$$I_T(v_x) = [A/(A+k_qn)](1+b)(M/e) \times \int_{v_z=0}^{v^{\max}}\int_{v_y=-v^{\max}}^{v^{\max}} j_A(z,\epsilon)Q_A^{\mathrm{H}\alpha}(\epsilon) \times N[v_z^b/(v_x^2+v_y^2+v_z^2)^{(1+b)/2}]dv_z dvy, \tag{10}$$

where the energy of the fast H atom is $\epsilon = M(v_x^2+v_y^2+v_z^2)/(2e)$, its maximum velocity is $v^{\max} = \sqrt{(2eV_0/M)}$, and V_0 is the voltage between the electrodes. One uses $v_x = \delta\lambda \times c/\lambda_0$ to convert to a wavelength shift.

B. Doppler model example

A representative Doppler profile calculated for viewing parallel to the electric field is shown in Fig. 12 for $E/N = 10$ kTd and 0.14 Torr, i.e., the data of Fig. 1 in Ref. [1]. In part (a) one sees the calculated excitation by fast H atoms and fast H_2 molecules moving toward cathode, the excitation by reflected fast atoms moving away from cathode, and the excitation of the line core by electrons and fast neutrals. Roughly 25% of the integrated central peak or line core ($\Delta\lambda < 0.2$ nm) is the result of the dissociative excitation of H_2 by H discussed in Sec. III G. Note that on the basis in Ref. [107], we have assumed that half of the dissociative excitation by electrons and all of the dissociative excitation by H and H_2 results in H($n=3$) with an effective temperature of 2.8 eV. The narrow portion of the profile attributed to electron excitation is plotted with a width roughly equal to the full spread of the Stark components. The contributions resulting from excitation by H^+, H_2^+, and H_3^+ are too small to show. The use of our earlier [42] recommended cross sec-

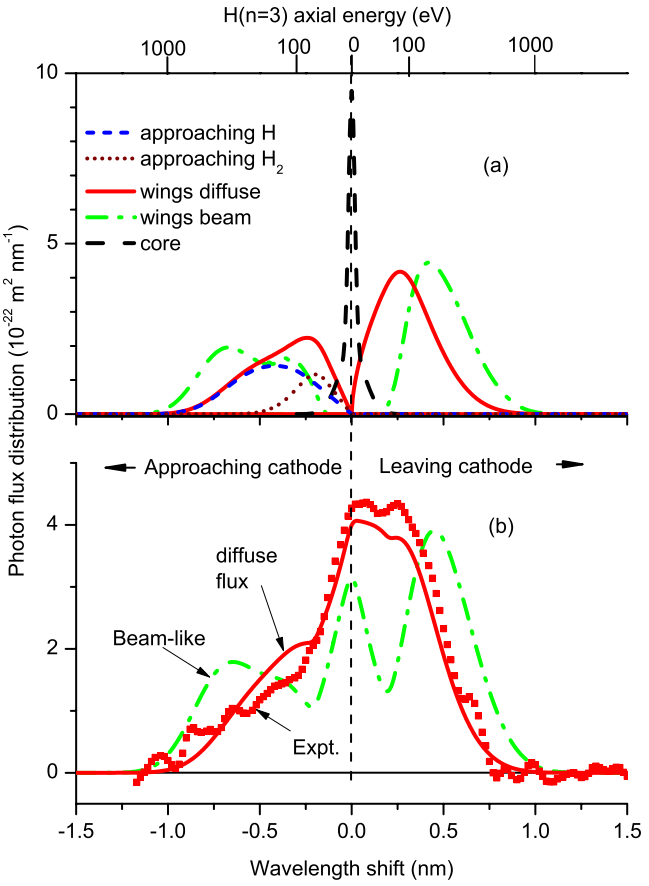

FIG. 12. (Color online) H_α Doppler profiles versus wavelength shift viewed along the electric field for $E/N=10$ kTd and 0.14 Torr. The upper scale is the H($n=3$) axial energy corresponding to the Doppler shift. (a) Components of calculated H_α Doppler profile for AuPd cathode. The solid (red) curves show the contributions of fast H and H_2 with assumed diffuse (see text) angular distributions for H($n=3$) atoms approaching (negative shifts) and leaving the cathode (positive shifts). The single-link chain (green) curves show the calculated emission for beamlike angular distributions. (b) Experimental profile for AuPd cathode (points) and calculated profiles (solid curves) for assumed diffuse and beamlike angular distributions. These calculated curves have been folded into the experimental instrument function of 0.2 nm FWHM.

tion for H_α excitation by H_2 increases the predicted emission for wavelength shifts between −0.5 and 0.0 nm by about a factor of 3 and appears contrary to experiment.

The peak of the component of the Doppler profile attributed to reflected H atoms in Fig. 12 is larger than that produced by the particles approaching the cathode because of the larger spatial extent of the emission by reflected atoms as shown in Fig. 7(b). The reflected atom component peaks at smaller $\Delta\lambda$ than for the approaching portion because of the lower energies of the reflected H atoms. For the conditions of this profile, the integrated intensity calculated for the component of the H_α profile excited by electrons is significantly smaller than the contributions of heavy-particle excitation, as is also evident from the spatial distributions shown in Fig. 7.

The solid red curve for negative $\Delta\lambda$ shows the excitation by fast H and H_2 approaching the cathode calculated assuming that these particles have a diffuse angular distribution, i.e., $b=1$ or a half width at half maximum (HWHM) of 60°. According to our assumed collisional excitation models, the nonisotropic component of the velocity distribution of the H($n=3$) atoms produced by fast atoms and molecules is the same as that of the incident atom or molecule. This causes the excitation by H_2 to appear much closer to line center than the excitation by H atoms. The dotted-dashed olive curve for negative $\Delta\lambda$ shows this sum calculated when these particles have a more beamlike ($b=100$ or HWHM=6.7°) angular distribution. The solid red curve for positive $\Delta\lambda$ shows the excitation by fast H leaving the cathode calculated assuming $b=0.6$. The dashed-dotted olive curve at positive $\Delta\lambda$ shows the component produced by reflected H atoms assuming the beamlike angular distribution ($b=100$).

In Fig. 12(b) we compare the sums of the components of Fig. 12(a), i.e., the calculated total H_α profiles, with the measured relative Doppler profile from Fig. 1 in Ref. [1] for a AuPd cathode. The experimental data are scaled in magnitude to fit the calculation. This signal is very noisy because of the very small power radiated at H_α by the low-current discharge, e.g., $\sim 4\times 10^{-4}$ W. The calculated sums of the components have been folded into a triangular function with a full width half maximum (FWHM) of 0.2 nm to simulate the instrument function. As indicated in Sec. III J, our choice of a lower dissociative excitation cross section at low energies for H_2+H_2 collisions reduces the discrepancy between the calculated and measured profiles at $\Delta\lambda\sim -0.3$ nm by about 1/2. In view of the poor signal to noise ratio, this is a tentative argument.

In Fig. 12(b), we also show the effect of changes in the assumed angular distribution of H($n=3$) atoms excited by fast H atoms approaching the cathode. A considerable improvement in agreement with experiment results from the assumption of a distribution given by Eq. (8) with $b=1$, as compared to the result with $b=100$. This somewhat surprising improvement has led us to adopt $b=1$ as our "standard" model for H($n=3$) atoms approaching the cathode along with $b=0.6$ for H($n=3$) atoms leaving the cathode. Obviously, there is a need for a more exact kinetics model, including the application of the largely unknown energy-dependent differential scattering cross sections for collisions of H, H^+, H_2^+, H_3^+, and H_2 with H_2 and collisions with the wall.

We recognize that our choice of a diffuse angular distribution is not a unique solution to fitting the low velocity portion of the H_α Doppler profile. An example of an alternate hypothesis is that our model results in a deficiency of low energy H($n=3$) atoms, as suggested by the comparison of calculated and measured ion energy distributions for H^+ in Fig. 9. An argument for the approximate validity of our standard model for our range of pressure and electrode separations is the totality of the agreement between the model and experiment. For example, if the energy distributions for H($n=3$) and its precursors were lowered to energies nearer the excitation threshold, the agreement of the model and experiment for the absolute excitation cross sections shown in Figs. 7 and 8 would be expected to fail.

VI. NEAR-UV CONTINUUM OF H_2

In this section we apply the model of the present paper to the determination of the cross section for excitation of the

near-uv continuum shown in Fig. 5. Figure 10 in Ref. [2] shows comparisons of calculated and measured spatial distributions of H_2 near-uv continuum emission for E/N from 300 Td to 10 kTd obtained using the ion and fast atom model developed in this paper. The variation in the heavy particle and electron excitation portions of the continuum excitation with position, pressure, and E/N are qualitatively similar to that for the H_α excitation [2]. Collisional quenching is small ($\leq 10\%$) for our pressures [108,109]. Our proposed cross section Q_A^{uv} for the excitation of the $H_2(a^3\Sigma)$ state and its near-uv continuum by fast H atoms is adjusted to fit these data and is shown in Fig. 5. We note that at energies below a few hundred eV, this excitation cross section is much larger than that for the excitation of H_α by H atoms. We have not found published cross sections for the excitation of this continuum by hydrogen ions, atoms, or molecules.

VII. DISCUSSION

This paper recommends and tests against experiment a set of heavy-particle collision and reaction cross sections for use in modeling discharges in weakly ionized H_2. The comparisons of model predictions with experiment are particularly sensitive to cross sections in the energy range from a fraction of an eV to several hundred eV. In addition to the reaction cross sections for the various ions, our analysis brings out the importance of the cross sections for ion, atom, and molecule momentum transfer and the resultant energy loss by target recoil at low energies. For the higher energies, inelastic energy loss to excitation and ionization dominates. In the case of momentum transfer collisions by H^+, we merge low energy theory and higher energy experiment, but for H_3^+ at high energies we have only the scaling of the H^+ momentum transfer cross sections as a guide. The behavior of H_2^+ is dominated by H_3^+ formation at energies below about 10 eV and by symmetric charge transfer at higher energies.

The comparisons of calculated and measured spatial profiles presented in this paper have allowed us to estimate several unknown or poorly known cross sections. Thus, we obtained reasonable fits to the measured heavy-particle excitation of H_α at $E/N=350$ Td by scaling data from beam experiments for similar excitation processes so as to reduce the low energy portions of the H_α excitation cross sections in $H_2^+ + H_2$ and $H^+ + H_2$ collisions compared to those in Ref. [42]. On the other hand, fitting the measured near-uv continuum of H_2 yielded a surprisingly large excitation cross section in $H + H_2$ collisions at low energies. Cross sections for the breakup of H_3^+ in collisions with H_2 are updated from our earlier compilation [42]. In the sequence leading to H_α excitation in $H_2 + H_2$ collisions, it is necessary to estimate several cross sections. Obviously, direct measurements of such unknown or poorly known cross sections are desirable. Preliminary models [110] that take into account the angular scattering are in need of realistic differential scattering data. The comparison of experiment with our model in this paper also points to the need for the use of better models [111,112] of electron behavior at very high E/N.

Our model shows that for electron-produced weakly ionized hydrogen discharges in a uniform electric field there is a transition of the dominant ion at the cathode from H_3^+ at low E/N to H^+ at intermediate E/N and to H_2^+ at the highest E/N. Heavy-particle excitation of H_α and of the near-uv continuum of H_2 is found to be dominated by fast H atoms produced by charge transfer from H^+. The model predicts some H_α excitation by fast H_2 at high E/N. Excitation by ions is calculated to be small for all of our conditions. We have also shown that the prediction of the model of H_α excitation by fast ground state H atoms leaving the cathode is in much better agreement with experiment than in a model in which the excited H atoms are produced at the cathode surface.

We are unable to obtain good agreement with published ion-flux energy distributions or with energy-integrated fluxes for H^+ and H_3^+, although the agreement for H_2^+ is satisfactory. One possibility is that the direct measurements of ion energy distributions are more reliable when the angular distribution of the ions is more forward peaked as the result of nearly complete energy loss on collision, as occurs with large cross sections for symmetric charge transfer collisions of H_2^+ with H_2. Thus, the persistence of the projectile velocity may make the ion optics less reliable. Our attempts to improve the agreement between the model and experiment by adding large energy losses for H^+ and H_3^+ to the model do not look promising.

The model presented in this paper is greatly simplified with respect to the Boltzmann equation used to describe the charged and neutral particle reactions and their transport and with respect to the computational techniques used to solve the Boltzmann equations. These approximations allowed the author to concentrate on improving the reaction and transport cross sections and on comparison of model predictions with experiment. The generation and inclusion of differential scattering cross sections and the use of better computational approaches are essential to the improvement of future models. The comparisons of our model to Doppler profile experiments [3] provide evidence that our beam model underestimates the effects of angular scattering in heavy-particle collisions with H_2. Thus, the shape of the wing of the Doppler profile corresponding to fast atoms approaching the cathode agrees much better with experiment when a broad angular distribution is assumed for the fast excited atoms. Evidence that we are justified in separating the components approaching and leaving the cathode, i.e., that the angular distribution is far from isotropic, is the asymmetry in the Doppler profile for both the AuPd and graphite cathodes [3].

The model considerations of this paper suggest several experiments. One is the use of a drift tube with a highly transparent cathode, such as the grid electrode used with Ar [113]. This will greatly reduce the emission caused by reflected H atoms and enable a more careful study of H_α and H_2 near-uv buildup with distance from the anode. With a sufficiently small reflected H atom signal, it may be possible to observe the increase with pressure and particle scattering of a component of the H_α Doppler profile caused by $H(n=3)$ atoms moving opposite the direction of electric field acceleration. Second, the behavior of ions injected into a region with no electric field or a low electric field beyond the cathode would simulate more closely the excitation conditions proposed for planetary aurora [45–48], although miss-

ing the effects caused by collisions with atomic H. An additional possibility is a drift tube with a double grid for an anode, biased such that the electrons reaching the anode are stopped, allowing the H atoms reflected from the anode to enter a field free region. The presence and attenuation of H_α emission from $H+H_2$ collisions would test further the present model in the energy range not covered by beam experiments [60]. Another improvement in the drift-tube experiment would be to apply an axial magnetic field to reduce the suggested radial losses of electrons and improve the approximation to a one-dimensional experiment.

Measurements and simplified models of excitation by fast atoms and/or molecules at high E/N have now been published for low-current discharges in N_2 [88], Ar [102,113], He [114], and now in H_2. The magnitude of the fast particle excitation of H_α varies drastically with the cross sections for charge transfer and excitation by the various ions, atoms, and molecules [115].

We have briefly applied variations in this simplified model to several other experimental configurations. Application to moderate current density cathode fall experiments [30] yields H_α Doppler profiles, including the central core and both wings, and spatial distributions in rather good agreement with measurements using a copper cathode [29]. Unpublished application to a simplified model of electrostatic inertial confinement configurations leads to our suggestion that if the degree of H_2 dissociation is as small as usually assumed, the excitation of H_α by fast H atoms is more important than excitation by H^+ ions [33,34]. Our cross sections are expected to be applicable to models of emission from the auroras of the outer planets [31,32] and to models of fusion edge plasmas [50]. The quantitative successes of the present model of H_α emission from dc discharges support our previous criticism [35] of the interpretations of H_α production and line broadening observations from discharges that have been cited [37,38] as evidence for the production of hydrinos in a "resonance transfer" process. Basically, we claim that many of the dc and rf experiments of Mills and collaborators [37,38] do not definitively separate the points of origin of the H_α emission relative to the regions of low and high electric fields.

ACKNOWLEDGMENTS

The author would like to acknowledge many hours of critical and constructive discussion of this research with A. Gallagher. He thanks Z. Lj. Petrović, B. M. Jelenković, and A. Bogaerts for helpful discussions and Z. Lj. Petrović and V. Stojanović for providing results of their Monte Carlo model. This work was supported in part by JILA.

APPENDIX A: ELECTRON RATE COEFFICIENTS

In the present model we are primarily concerned with the ions and excited states produced by electrons and not with improved modeling the behavior of the electrons themselves. We therefore use a very simple fluid model in which the electrons leaving the cathode ionize and excite the H_2 at a constant rate after passing through a nonequilibrium region

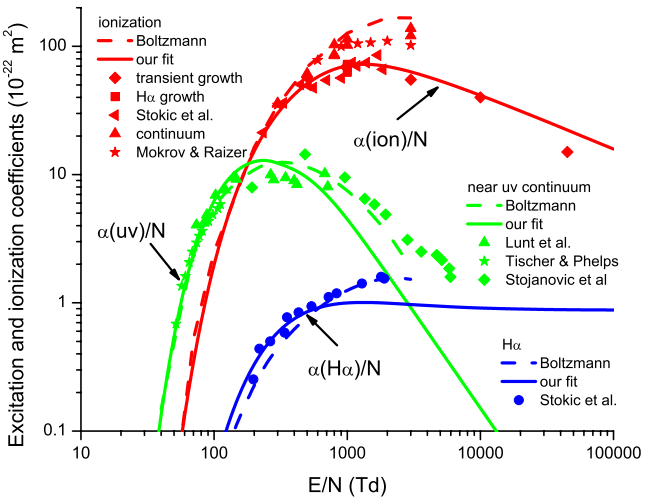

FIG. 13. (Color online) Excitation and ionization coefficients for electrons in H_2. The points attributed to Refs. [124,125] show relative excitation coefficients.

[5]. The quasiequilibrium ionization and excitation coefficients are presented as analytical expressions chosen to be consistent with the experiments presented in Ref. [2] as a whole rather than with individual experiments. This distinction arises from the fact that by adjusting the electron ionization and excitation coefficients used to model individual experiment, the fits of calculated to measured spatial distributions of emission can often be noticeably improved. We do not test for consistency between the ionization coefficients versus E/N, the Nd values, and the secondary electron yields at the cathode that are required for discharge maintenance in the very-low current or Townsend mode [5,9,116]. For comparison purposes, the ionization and excitation coefficients are calculated using the two-term Boltzmann equation with traditional electron-H_2 cross-section sets [52,53]. We have not tested for consistency with recent cross-section compilations [117,118]. Except as noted for our highest E/N, we assume that the effects of electron reflection from the graphite anode can be neglected [88].

Excitation and ionization coefficients for electrons in H_2 are shown in Fig. 13. Our empirical fit to theory and experiment for the spatial (Townsend) ionization coefficient α_i normalized to the gas density N is

$$\alpha_i/N = 1.0 \times 10^{-20} \exp[-405/(E/N)]/[(1 + \{(E/N)/1000\}^3)^{0.145}], \quad \text{(A1)}$$

where α_i/N is in m^2 and E/N is in Td. At $E/N < 300$ Td, our fit agrees with the Boltzmann equation results [52,53]. It should be kept in mind that we when we use the Townsend avalanche model at our higher E/N we are extrapolating the utility of the spatial ionization coefficient and the associated "local-field" model to higher E/N values than is usually considered valid [112,119]. Monte Carlo calculations [111,112,120] show an approximately exponential growth of electron current but only extend to $E/N=3$ kTd. Our choice for the empirical ionization coefficient is consistent with unpublished measurements of current growth [4,120]. At the

very highest E/N, α_i/N has been chosen so as to increase the ion production and the resultant H_α signal shown in Fig. 3 in Ref. [2]. We have taken the spatial ionization coefficient for the production of H^+ from theory and electron beam measurements [121], where it is ≈7% of that for H_2^+. From Fig. 13, an obvious concern is the tendency of the H_α emission experiments at our higher E/N to yield lower ionization coefficients than determined by other techniques.

Our empirical fit to the normalized spatial (Townsend) excitation coefficient α_x/N for the production of H_α by electrons shown by the solid curve of Fig. 13 is

$$\alpha_x/N = (2.75 \times 10^{-22} \exp[-400/(E/N)] - 1.88 \times 10^{-22} \times \exp\{-[800/(E/N)]\}), \quad \text{(A2)}$$

where α_x/N is in m^2. Here we note that our use of the Boltzmann equation result [52,53] for calibration of the H_α emission is in a range of E/N where the local-field model works well [119,122]. At $E/N < 500$ Td, our fitted excitation coefficient agrees with more recent experiments [39] but not with older data [123] (not shown). At our highest E/N, Eq. (A2) is chosen to fit the electron-dominated emission data near the anode at the low pressures shown in Ref. [2]. This procedure leads to an unexpected and unexplained slow variation in the effective excitation coefficient with E/N. These choices have no effect on the calibration procedure in Ref. [2] at low E/N. As for ionization, we have no firm explanation for the large spread in H_α excitation coefficients shown in Fig. 13.

Figure 13 also shows the electron excitation coefficient α_{uv}/N for the near-uv continuum of H_2. For $E/N < 100$ Td the analytic fit is based on calculations using the two-term Boltzmann equation. In this calculation, we neglect cascading from higher triplet states of H_2 and use the electron excitation cross section in Refs. [52,53]. The calculated variation for $E/N < 500$ Td is consistent with the relative measurements [124,125] shown. For $E/N > 300$ Td our empirical fit is adjusted primarily to fit the relative spatial distributions in Ref. [2]. It becomes significantly lower than the results of Stojanović *et al.* [126] at the higher E/N. Our fit is

$$\alpha_{uv}/N = \begin{cases} 3.3 \times 10^{-19} \exp[-330/(E/N)]/[1 + (E/N)/25]^2[1 + (E/N)/315] & \text{for } E/N \le 300 \text{ Td} \\ 1.35 \times 10^{-21}/\{1 + [(E/N)/500]^3\}^{0.5} & \text{for } E/N > 300 \text{ Td}. \end{cases} \quad \text{(A3)}$$

In our model of the nonequilibrium region near the cathode, we adopt the common approximation [5] that after electrons from the cathode traverse a voltage V_c the effective ionization coefficient is constant. Our assumed voltage is $V_c = 26 - 11(1 - \exp[-(500/(E/N))^2])$ V for E/N in Td and is based on experiments [116] and Monte Carlo results [112]. Current-growth experiments with this drift tube suggest larger values [4]. The assumed voltage traversed prior to excitation, i.e., 18 V, is consistent with known vertical excitation potentials for H_2 and with spatial scans H_α of emission at low pressures as reported in Ref. [2].

The magnitudes of the predicted spatially dependent excitation by ions and fast atoms at low and moderate E/N are rather weakly dependent on the effective ionization coefficient. This is understood by noting that when the multiplication is large compared to unity, as in Fig. 8, approximately one ion is produced in the gap per electron reaching the anode. Increasing the ionization coefficient causes the ions to be produced closer to the anode and results in relatively small changes in the effective length of the drift tube. As a result, the magnitude of the pronounced minimum in the observed H_α excitation versus distance is determined largely by the electron induced H_α excitation. This electron induced component near midgap is exponentially sensitive to the value of the ionization coefficient, with a smaller ionization coefficient leading to a larger minimum in the normalized H_α signal.

The effect of changes in the assumed ionization coefficient α_i/N on the spatially dependent H_α emission is rather different at high E/N and the accompanying low pressures, where few ions are produced per unit total current. Under these conditions, the ion production and apparent cross section for H_α production is approximately proportional to the assumed α_i/N. The existence of a steady-state discharge with such a low electron multiplication implies a large effective secondary electron yield [9,21].

APPENDIX B: H_α EMISSION NEAR CATHODE

In this appendix we are concerned with the effect of the finite radiative lifetime of the $H(n=3)$ atoms on the spatial distribution of the H_α emission that results from heavy-particle collisions. We explore this question using an approximate fluid model with sources representing production of $H(n=3)$ atoms at the cathode and production in gas phase collisions. The one-dimensional steady-state rate equation for the excited H atom density $n_X(z)$ is then

$$v_z dn_X(z,\epsilon)/dz = -An_X(z,\epsilon) - k_q N n_X(z,\epsilon) + j_R(\epsilon) Q_A^{H\alpha}(\epsilon) N, \quad \text{(B1)}$$

where j_R is flux of H atoms leaving the cathode, z is the distance from the cathode parallel to the electric field, and $v_z = \cos\theta\sqrt{(2e\epsilon/M)}$ is the z component of the reflected fast $H(n=3)$ atom velocity traveling at an angle θ relative to the discharge axis for a H atom of mass M and energy ϵ in eV. The effective radiative transition probability A for the $H(n=3)$ state is assumed to be 10^8 s^{-1} in the presence of strong level mixing by the applied electric field [85]. The effective rate coefficient for collisional quenching k_q is assumed to

have the energy independent value of 5×10^{-15} m^3 s^{-1} found in Sec. IVA in Ref. [2]. The cross section $Q_A^{H\alpha}(\epsilon)$ for excitation of H_α in collisions of fast H with H_2 is that given in Fig. 5. Angular scattering and loss of ground state H atoms are neglected for the short distance times pressure involved.

The solution to Eq. (B1) is

$$n_X(z,\epsilon) = n_X(0,\epsilon)\exp(-z/z_0) + j_R(\epsilon)Q_A^{H\alpha}(\epsilon)N/(A+k_qN)[1-\exp(-z/z_0)], \tag{B2}$$

where $z_0=v_z/(A+k_qN)$. The first term represents the excitation of H_α as the result of collisions of fast H or H^+ with the cathode surface such that $n_X(0,\epsilon)=\Sigma_i e_i j_i/v_z$, where the j_i are the fluxes of Sec. IV A. The surface excitation efficiencies e_i for H_α are expected to be smaller than those measured [127] for H^+ excitation of Lyman α, i.e., $\sim10^{-3}$. For the conditions of Fig. 7, application of Eq. (B2) means that the maximum value of the first term is less than about 10% of the second. The decay and/or buildup of H_α emission with a characteristic distance $z_0\sim1$ mm predicted by Eq. (B2) would be very difficult to detect in the presence of electron-nonequilibrium and finite-spatial-resolution effects near the cathode and the noise in the signal. These estimated magnitudes are verified by extending the numerical analysis of Sec. IV A to include an equation similar to Eq. (6) for the H($n=3$) excited state flux. As argued in Ref. [1], extension of these models to glow discharges [30] leads to inconsistencies with the proposal by Barbeau and Jolly [12] that their observed H_α intensity from H($n=3$) leaving the cathode results from excited atom production at the cathode surface and subsequent radiative and collisional destruction.

[1] Z. Lj. Petrović, B. M. Jelenković, and A. V. Phelps, Phys. Rev. Lett. **68**, 325 (1992).
[2] Z. Lj. Petrović and A. V. Phelps (unpublished).
[3] Z. Lj. Petrović and A. V. Phelps (unpublished).
[4] Z. Lj. Petrović and A. V. Phelps (unpublished).
[5] M. J. Druyvesteyn and F. M. Penning, Rev. Mod. Phys. **12**, 87 (1940).
[6] G. Francis, Handb. Sens. Physiol. **22**, 53 (1956).
[7] Yu. P. Raizer, *Gas Discharge Physics* (Springer-Verlag, Berlin, 1991), Chap. 8.
[8] A. V. Phelps, Z. Lj. Petrović, and B. M. Jelenković, Phys. Rev. E **47**, 2825 (1993).
[9] A. V. Phelps and Z. Lj. Petrović, Plasma Sources Sci. Technol. **8**, R21 (1999).
[10] A. V. Phelps, J. Appl. Phys. **76**, 747 (1994).
[11] E. Hantzsche, Beitr. Plasmaphys. **9**, 439 (1969).
[12] C. Barbeau and J. Jolly, J. Phys. D **23**, 1168 (1990).
[13] K. G. Emeleus and J. R. M. Coulter, J. Phys. D **16**, 2181 (1983).
[14] A. C. Dexter, T. Farrel, and I. M. Lees, J. Phys. D **22**, 413 (1989).
[15] D. Heim and H. Störi, J. Appl. Phys. **72**, 3330 (1992).
[16] T. Šimko, V. Martišovitš, J. Bretagne, and G. Gousset, Phys. Rev. E **56**, 5908 (1997).
[17] D. L. Albritton, T. M. Miller, D. W. Martin, and E. W. McDaniel, Phys. Rev. **171**, 94 (1968).
[18] T. M. Miller, J. T. Moseley, D. W. Martin, and E. W. McDaniel, Phys. Rev. **173**, 115 (1968).
[19] J. Bretagne, G. Gousset, T. Šimko, M. V. V. S. Rao, R. J. Van Brunt, Y. Wang, J. K. Olthoff, B. L. Peko, and R. L. Champion, Europhys. Conf. Abstr. **20E**, 115 (1996). Although the ion energy distributions cited by these authors for $E/N=1$ kTd, $p=0.46$ Torr, and $d=2$ cm are presumably obtained with the same apparatus as those cited by Rao *et al.* [89], they differ significantly.
[20] J. Bretagne, G. Gousset, and T. Šimko, J. Phys. D **27**, 1866 (1994).
[21] T. Ŝimko, J. Bretagne, and G. Gousset, in *Proceedings of the XXIII International Conference Physics of Ionized Gases*, edited by M. C. Bordage and A. Gleizes (EDP Sciences, Toulouse, 1996), p. IV-184.
[22] G. W. McClure and K. D. Granzow, Phys. Rev. **125**, 3 (1962).
[23] G. W. McClure, Phys. Rev. **130**, 1852 (1963).
[24] R. Johnsen, C.-M. Huang, and M. A. Biondi, J. Chem. Phys. **65**, 1539 (1976).
[25] A. L. Cappelli, R. A. Gottscho, and T. A. Miller, Plasma Chem. Plasma Process. **5**, 317 (1985).
[26] E. L. Ayers and W. Benesch, Phys. Rev. A **37**, 194 (1988).
[27] B. P. Lavrov and A. S. Melinkov, Opt. Spektrosk. **75**, 1152 (1993) [Opt. Spectrosc. **75**, 676 (1993)]; **79**, 922 (1995); [Opt. Spectrosc. **79**, 842 (1995)].
[28] S. B. Radovanov, K. Dzierżęga, J. R. Roberts, and J. K. Olthoff, Appl. Phys. Lett. **66**, 2637 (1995).
[29] N. Cvetanović, M. N. Kuraica, and N. Konjević, J. Appl. Phys. **97**, 033302 (2005); M. R. Gemišić Adamov, B. M. Orbradović, M. M. Kuraica, and N. Konjević, IEEE Trans. Plasma Sci. **31**, 444 (2003).
[30] A. V. Phelps, Bull. Am. Phys. Soc. **53**, 41 (2008).
[31] N. Achilleos, S. Miller, J. Tennyson, A. D. Aylward, I. Mueller-Wodarg, and D. Rees, J. Geophys. Res. **103**, 20089 (1998).
[32] J. J. Perry, Y. H. Kim, J. L. Fox, and H. S. Porter, J. Geophys. Res. **104**, 16541 (1999).
[33] O. Shrier, J. Khachan, S. Bosi, M. Fitzgerald, and N. Evans, Phys. Plasmas **13**, 012703 (2006).
[34] See, for example, J. D. Hey, C. C. Chu, Ph. Mertens, S. Brezinsek, and B. Unterberg, J. Phys. B **37**, 2543 (2004); R. J. Kanzleiter, D. P. Stotler, C. F. F. Karney, and D. Steiner, Phys. Plasmas **7**, 5064 (2000).
[35] A. V. Phelps, J. Appl. Phys. **98**, 066108 (2005).
[36] H.-J. Kunze, J. Phys. D **41**, 108001 (2008).
[37] R. L. Mills, B. Dhandapani, and K. Akhtar, Int. J. Hydrogen Energy **33**, 802 (2008), and references therein.
[38] J. Phillips, C. K. Chen, and R. L. Mills, Int. J. Hydrogen Energy **33**, 2419 (2008), and references therein.
[39] Z. Stokic, M. M. F. R. Fraga, J. Bozin, V. Stojanovic, Z. Lj. Petrović, and B. M. Jelenković, Phys. Rev. A **45**, 7463 (1992).
[40] A. V. Phelps (unpublished). Analytic formulas for cross sections used in the present paper and for some related differential cross sections are available on request to avp@jila.colorado.edu
[41] The calculated numbers of momentum transfer collisions for

H^+, H_2^+, and H_3^+ with H_2 for the conditions of Fig. 1(a) are 0.3, 2 (0.4), and 0.3, respectively. For Fig. 1(b), they are 56, 0.6 (2.2), and 62, respectively. The numbers in parentheses are the numbers of low energy ion conversion reactions for H_2^+ to H_3^+, which dominate the higher energy elastic scattering for H_2^+ at low E/N. Such numbers for H and H_2 are not very meaningful because of their large fluxes at very-low energy.

[42] A. V. Phelps, J. Phys. Chem. Ref. Data **19**, 653 (1990); **20**, 1339 (1991); **23**, 153 (1994).

[43] T. Tabata and T. Shirai, At. Data Nucl. Data Tables **76**, 1 (2000).

[44] A. Bogaerts and R. Gijbels, Spectrochim. Acta, Part B **57**, 1071 (2002); J. Anal At. Spectrom. **17**, 768 (2002).

[45] A. Bhardwaj and R. P. Singhal, J. Geophys. Res. **98**, 9473 (1993).

[46] D. Rego, R. Prangé, and J.-C. Gérard, J. Geophys. Res. **99**, 17075 (1994).

[47] D. V. Bisikalo and V. I. Shematovich, J. Geophys. Res. **101**, 21157 (1996).

[48] S. Miller, T. Stallard, C. Smith, G. Millward, H. Melin, M. Lystrup, and A. Aylward, Philos. Trans. R. Soc. London **364**, 3121 (2006).

[49] T. Okuno, At. Plasma-Mater. Interact. Data Fusion **10**, 163 (2002). We note that most of these cross sections decrease rapidly compared to ours at energies above about 5 eV.

[50] D. Reiter, V. Kotov, P. Börner, K. Sawada, R. K. Janev, and B. Kuppers, J. Nucl. Mater. **363-365**, 649 (2007).

[51] R. K. Janev, D. Reiter, and U. Samm (unpublished). Available at http://www.eirene.de/reports/report_4105.pdf; an earlier compilation is R. K. Janev, W. D. Langer, K. Evans, and D. E. Post, *Elementary Processes in Hydrogen-Helium Plasmas* (Springer-Verlag, Berlin, 1985).

[52] S. J. Buckman and A. V. Phelps, J. Chem. Phys. **82**, 4999 (1985).

[53] A. V. Phelps (unpublished). See files in the directories ElectronNeutral and IonNeutral at ftp:/jila.colorado.edu/collision_data/

[54] J. K. Kim, L. P. Thread, and W. T. Huntress, Jr., Int. J. Mass Spectrom. Ion Phys. **15**, 223 (1974).

[55] V. G. Anicich and J. H. Futrell, Int. J. Mass Spectrom. Ion Process. **55**, 189 (1984).

[56] The increase in ion-molecule reaction rates caused by a buildup of internal energy for N_2^+ drifting through He at high E/N has been discussed by M. Kriegel, R. Richter, W. Lindinger, L. Barbier, and E. E. Ferguson, J. Chem. Phys. **88**, 213 (1988); **91**, 4426 (1989).

[57] P. S. Krstić and D. R. Schultz, J. Phys. B **32**, 2415 (1999).

[58] K. A. Smith, L. K. Johnson, R. S. Gao, and R. F. Stebbings, in *Abstracts of Contributed Papers for International Conference on the Physics of Electronic and Atomic Collisions*, edited by J. Geddes, H. B. Gilbody, A. E. Kingston, C. J. Latimer, and H. R. J. Walters (North-Holland, Amsterdam, 1987), p. 681; J. H. Newman, Y. S. Chen, K. A. Smith, and R. F. Stebbings, J. Geophys. Res. **91**, 8947 (1986); **94**, 7019 (1989); R. S. Gao, L. K. Johnson, G. J. Smith, C. L. Hakes, K. A. Smith, N. F. Lane, R. F. Stebbings, and M. Kimura, Phys. Rev. A **44**, 5599 (1991); R. F. Stebbings (private communication).

[59] B. Van Zyl, M. W. Gealy, and H. Neumann, Phys. Rev. A **40**, 1664 (1989).

[60] I. D. Williams, J. Geddes, and H. B. Gilbody, J. Phys. B **15**, 1377 (1982).

[61] W. R. Hess, Phys. Rev. A **9**, 2036 (1974).

[62] A. E. S. Green and L. R. Peterson, J. Geophys. Res. **73**, 233 (1968).

[63] W. Eckstein and J. P. Biersack, Appl. Phys. A: Solids Surf. **38**, 123 (1985).

[64] W. Eckstein and H. Verbeek, in *Data Compendium for Plasma-Surface Interactions*, edited by R. A. Langley, J. Bohdansky, W. Eckstein, P. Mioduszewski, J. Roth, E. Taglauer, E. W. Thomas, H. Verbeek, K. L. Wilson (International Atomic Energy Agency, Vienna, Austria, 1984) p. 12.

[65] R. Aratari and W. Eckstein, Nucl. Instrum. Methods Phys. Res. B **42**, 11 (1989).

[66] T. Babkina, T. Gans, and U. Czarnetzki, Europhys. Lett. **72**, 235 (2005).

[67] We thank T. Gans for a helpful discussion of this point.

[68] G. M. McCracken, Rep. Prog. Phys. **38**, 241 (1975).

[69] J. E. Pollard, L. K. Johnson, D. A. Lichtin, and R. B. Cohen, J. Chem. Phys. **95**, 4877 (1991).

[70] C.-L. Liao, C.-X. Liao, and C. Y. Ng, J. Chem. Phys. **81**, 5672 (1984).

[71] It appears that Janev *et al.* [51] misinterpreted the measurement of reaction (3) in Ref. [128] as applying to $H_2^+ + H_2$ collisions rather than to $H_2^+ + H$ collisions.

[72] B. L. Peko and R. L. Champion, J. Chem. Phys. **107**, 1156 (1997).

[73] J. F. Williams and D. N. F. Dunbar, Phys. Rev. **149**, 62 (1966).

[74] The cross sections in Ref. [72] are still believed by its authors to be correct to within the stated accuracies, in contrast to what might be inferred from Ref. [16]. R. L. Champion (private communication).

[75] B. A. Huber, U. Schulz, and K. Wiesemann, Phys. Lett. **79A**, 58 (1980).

[76] W. Brandt, A. Ratkowski, and R. H. Ritchie, Phys. Rev. Lett. **33**, 1325 (1974); E. Ray, R. Kirsch, H. H. Mikkelsen, J. C. Poizat, and J. Remillieux, Nucl. Instrum. Methods Phys. Res. B **69**, 133 (1992). Because of extrapolation of the energy loss from the solid phase to gases, our estimate is expected to be very rough.

[77] B. Van Zyl and H. Neumann, J. Geophys. Res. **85**, 6006 (1980); B. Van Zyl, M. W. Gealy, and H. Neumann, Phys. Rev. A **28**, 176 (1983).

[78] V. T. Chiplonkar, Proc. Natl. Inst. Sci. India **7**, 103 (1941).

[79] B. L. Preppernau, K. Pearce, A. Tserepi, E. Wurzberg, and T. A. Miller, Chem. Phys. **196**, 371 (1995).

[80] K. Niemi, V. Schulz-von der Gathen, and H. F. Döbele, J. Phys. D **34**, 2330 (2001).

[81] J. Bittner, K. Kohse-Höinghaus, U. Meier, and Th. Just, Chem. Phys. Lett. **143**, 571 (1988).

[82] A. Catherinot, B. Dubreuil, and M. Gand, Phys. Rev. A **18**, 1097 (1978).

[83] J. W. L. Lewis and W. D. Williams, J. Quant. Spectrosc. Radiat. Transf. **16**, 939 (1976).

[84] R. H. Hughes and H. Kisner, Phys. Rev. A **5**, 2107 (1972).

[85] C. C. Havener, N. Rouze, W. B. Westerveld, and J. S. Risley, Phys. Rev. A **33**, 276 (1986).

[86] Rated as "semiconductor" grade fused silica. The reflection coefficient for 100 eV D atoms striking graphite at angles of ~70° to the normal is ~0.8 for a smooth surface compared to ~0.4 for a rough surface. See M. Mayer, W. Eckstein, and B.

M. U. Scherzer, J. Appl. Phys. **77**, 6609 (1995) We have found no data for reflection at a fused silica surface.
[87] I. D. Williams, J. Geddes, and H. B. Gilbody, J. Phys. B **16**, L765 (1983).
[88] B. M. Jelenković and A. V. Phelps, Phys. Rev. A **36**, 5310 (1987).
[89] M. V. V. S. Rao, R. J. Van Brunt, and J. K. Olthoff, in Abstracts of International Symposium on Electron- and Photon-Molecule Collisions and Swarms, edited by T. N. Rescigno, Berkeley, CA, 1995 (unpublished), p. H-9.
[90] A. V. Phelps, B. M. Jelenković, and L. C. Pitchford, Phys. Rev. A **36**, 5327 (1987).
[91] T. E. Madey and J. T. Yates, Jr., J. Vac. Sci. Technol. **8**, 525 (1971).
[92] E. W. McDaniel, *Collision Phenomena in Ionized Gases* (Wiley, New York, 1964) (Eq. 1-5-9).
[93] R. E. Johnson, *Introduction to Atomic and Molecular Collisions* (Plenum, New York, 1982), p. 38.
[94] K. G. Muller and P. Wahle, Z. Phys. **179**, 52 (1964).
[95] G. N. Hays, L. C. Pitchford, J. B. Gerardo, J. T. Verdeyen, and Y. M. Li, Phys. Rev. A **36**, 2031 (1987).
[96] H. A. Bethe and E. E. Saltpeter, *Quantum Mechanics of One- and Two-Electron Atoms* (Academic, New York, 1957), p. 284.
[97] T. L. Kwok, S. Guberman, A. Dalgarno, and A. Posen, Phys. Rev. A **34**, 1962 (1986).
[98] Z. Lj. Petrović and A. V. Phelps, in *Proceedings of the International Seminar on Reactive Plasmas*, edited by T. Goto (Nagoya University, Nagoya, 1991), p. 351.
[99] The discrepancy between the model and experiment for distances larger than 0.02 m in Fig. 8 is easily removed by increasing the empirical electron excitation coefficient α_x/N of Appendix by about a 15%. We have left such discrepancies uncorrected in favor of a smooth dependence of the excitation coefficient on E/N.
[100] M. V. V. S. Rao, R. J. Van Brunt, and J. K. Olthoff, Phys. Rev. E **54**, 5641 (1996).
[101] Analytic solutions have been obtained to the partial differential equations for H^+, H_2^+, and H_3^+ for simplified cross sections, e.g., constant reaction cross sections, and for conditions appropriate to $E/N=10$ kTd, e.g., small energy loss for H^+ and H_3^+. These results show a flat behavior of the flux energy distributions for H^+ and H_3^+ at low energies, such as shown in Fig. 9 for H^+. This is in contrast to the sharp peak at low energies shown in some experimental ion energy distributions [19] for H^+ and H_3^+. A relatively flat energy distribution at low energies has been obtained by Petrović and Stomatović for H^+ and H_3^+ at $E/N=10$ kTd using a Monte Carlo solution [110].
[102] A. V. Phelps and B. M. Jelenković, Phys. Rev. A **38**, 2975 (1988).
[103] J. Fletcher and H. A. Blevin, J. Phys. D **14**, 27 (1981).
[104] J. A. Ray, C. F. Barnett, and B. Van Zyl, J. Appl. Phys. **50**, 6516 (1979).
[105] C. Stehlé, J. Quant. Spectrosc. Radiat. Transf. **44**, 135 (1990).
[106] J. F. Kielkopf, J. Chem. Phys. **62**, 3784 (1975).
[107] R. S. Freund, J. A. Schiavone, and D. F. Brader, J. Chem. Phys. **64**, 1122 (1976); K. Ito, N. Oda, Y. Hatano, and T. Tsuboi, Chem. Phys. **21**, 203 (1977).
[108] R. E. Center, J. Chem. Phys. **54**, 3499 (1971).
[109] A. B. Wedding and A. V. Phelps, J. Chem. Phys. **89**, 2965 (1988).
[110] Z. Petrović and V. Stojanović, in *Proceedings of the Fifth Serbian Conference on Spectral Lines Shapes in Astrophysics*, edited by L. C. Popović and M. S. Dimitrijević (Memorie della Società Astronomica Italiana, Trieste, 2005), Vol. 7, p. 172.
[111] M. Hayashi, J. Phys. Colloq. **40**, C7-45 (1979).
[112] M. S. Mokrov and Yu. P. Raizer, Zh. Tekh. Fiz. **78**, 47 (2008) [Tech. Phys. **53**, 436 (2008)]; these recent Monte Carlo calculations of electron induced ionization in H_2 agree well with the experiments of M. A. Folkhard and S. C. Haydon, Aust. J. Phys. **24**, 527 (1970) at overlapping E/N of 300–700 Td.
[113] D. A. Scott and A. V. Phelps, Phys. Rev. A **43**, 3043 (1991).
[114] B. M. Jelenković and A. V. Phelps, Phys. Rev. E **71**, 016410 (2005).
[115] A. V. Phelps, J. Phys. Chem. Ref. Data **21**, 883 (1992).
[116] M. A. Folkhard and S. C. Haydon, Aust. J. Phys. **24**, 527 (1971).
[117] J.-S. Yoon, M.-Y. Song, J.-M. Han, S. H. Hwang, W.-S. Chang, B. J. Lee, and Y. Itikawa, J. Phys. Chem. Ref. Data **37**, 913 (2008).
[118] M. Brunger, R. S. Brusa, S. J. Buckman, M. T. Elford, Y. Hatano, Y. Itikawa, K. Kameta, G. P. Karwasz, N. Kouchi, B. G. Lindsay, M. A. Mangan, and A. Zecca, in *Photon and Electron Interactions with Atoms, Molecules and Ions*, edited by Y. Itikawa, Landolt-Börnstein, Group I, Vol. 17C (Springer, New York, 2003).
[119] For a review of recent advances see Z. Donkó, P. Hartmann, and K. Kutasi, Plasma Sources Sci. Technol. **15**, 178 (2006).
[120] One notes that the ionization coefficients derived from our spatially dependent emission data and from our transient data [4] are systematically lower than the recent Monte Carlo calculations of Mokrov and Raizer [112] and experiments such as those of Folkhard and Haydon [116]. If we were to raise our fit to the ionization coefficient data by, for example, ~1.5 at 3 kTd so as to fit the Monte Carlo result, we would need to correspondingly lower the reflected fast atom flux from our interpretation of surface experiments or to lower the cross section for excitation of $H(n=3)$ by H atoms from experiment. A possible reason for low apparent ionization and excitation coefficients in our drift tube is the loss of scattered electrons to the side walls of the drift tube [119].
[121] X. Liu and D. E. Shemansky, Astrophys. J. **614**, 1132 (2004).
[122] G. A. Baraff and S. J. Buchsbaum, Phys. Rev. **130**, 1007 (1963).
[123] K. J. Nygaard, Appl. Sci. Res., Sect. B **12**, 91 (1965).
[124] R. W. Lunt, C. A. Meek, and E. C. W. Smith, Proc. R. Soc. London, Ser. A **158**, 729 (1937).
[125] H. Tisher and A. V. Phelps (unpublished).
[126] V. Stojanović, J. Božin, Z. Stokić, Z. Lj. Petrović, and B. M. Jelenković, in *Proceedings of the Symposium on Atomic and Surface Physic*, edited by T. D. Mark and F. Howorka (Innsbruck, Universität Innsbruck, Obertraun, Austria, 1990), p. 160.
[127] Yu-Yuan R. Hsiao and R. C. Amme, Phys. Rev. A **20**, 214 (1979).
[128] Z. Karpas, V. Anicich, and W. T. Huntress, Jr., J. Chem. Phys. **70**, 2877 (1979).